NASA/TM-2005-213946
ARL-TR-3691

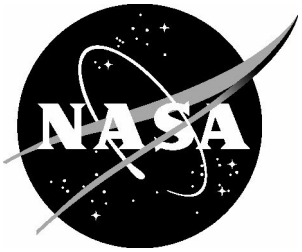

Flow Angularity Measurements in the NASA-Langley Transonic Dynamics Tunnel

William T. Yeager, Jr., Matthew L. Wilbur, Paul H. Mirick
U.S. Army Research Laboratory
Vehicle Technology Directorate
Langley Research Center, Hampton, Virginia

José A. Rivera, Jr.
Langley Research Center, Hampton, Virginia

December 2005

The NASA STI Program Office . . . in Profile

Since its founding, NASA has been dedicated to the advancement of aeronautics and space science. The NASA Scientific and Technical Information (STI) Program Office plays a key part in helping NASA maintain this important role.

The NASA STI Program Office is operated by Langley Research Center, the lead center for NASA's scientific and technical information. The NASA STI Program Office provides access to the NASA STI Database, the largest collection of aeronautical and space science STI in the world. The Program Office is also NASA's institutional mechanism for disseminating the results of its research and development activities. These results are published by NASA in the NASA STI Report Series, which includes the following report types:

- TECHNICAL PUBLICATION. Reports of completed research or a major significant phase of research that present the results of NASA programs and include extensive data or theoretical analysis. Includes compilations of significant scientific and technical data and information deemed to be of continuing reference value. NASA counterpart of peer-reviewed formal professional papers, but having less stringent limitations on manuscript length and extent of graphic presentations.

- TECHNICAL MEMORANDUM. Scientific and technical findings that are preliminary or of specialized interest, e.g., quick release reports, working papers, and bibliographies that contain minimal annotation. Does not contain extensive analysis.

- CONTRACTOR REPORT. Scientific and technical findings by NASA-sponsored contractors and grantees.

CONFERENCE PUBLICATION. Collected papers from scientific and technical conferences, symposia, seminars, or other meetings sponsored or co-sponsored by NASA.

- SPECIAL PUBLICATION. Scientific, technical, or historical information from NASA programs, projects, and missions, often concerned with subjects having substantial public interest.

- TECHNICAL TRANSLATION. English-language translations of foreign scientific and technical material pertinent to NASA's mission.

Specialized services that complement the STI Program Office's diverse offerings include creating custom thesauri, building customized databases, organizing and publishing research results ... even providing videos.

For more information about the NASA STI Program Office, see the following:

- Access the NASA STI Program Home Page at ***http://www.sti.nasa.gov***

- E-mail your question via the Internet to help@sti.nasa.gov

- Fax your question to the NASA STI Help Desk at (301) 621-0134

- Phone the NASA STI Help Desk at (301) 621-0390

- Write to:
  NASA STI Help Desk
  NASA Center for AeroSpace Information
  7121 Standard Drive
  Hanover, MD 21076-1320

NASA/TM-2005-213946
ARL-TR-3691

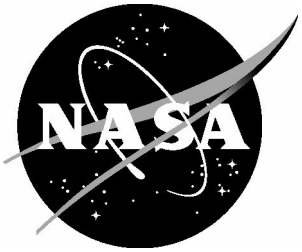

Flow Angularity Measurements in the NASA-Langley Transonic Dynamics Tunnel

William T. Yeager, Jr., Matthew L. Wilbur, Paul H. Mirick
U.S. Army Research Laboratory
Vehicle Technology Directorate
Langley Research Center, Hampton, Virginia

José A. Rivera, Jr.
Langley Research Center, Hampton, Virginia

National Aeronautics and
Space Administration

Langley Research Center
Hampton, Virginia 23681-2199

December 2005

Available from:

NASA Center for AeroSpace Information (CASI)
7121 Standard Drive
Hanover, MD 21076-1320
(301) 621-0390

National Technical Information Service (NTIS)
5285 Port Royal Road
Springfield, VA 22161-2171
(703) 605-6000

Abstract

An investigation using a survey rake with 11 five-hole pyramid-head probes has been conducted in the Langley Transonic Dynamics Tunnel (TDT) to measure the test section flow angularity. Flow measurements were made in a 10-ft square grid centered about the test section centerline at a single streamwise location for nine Mach numbers ranging from 0.50 to 1.19 at dynamic pressures of 100 and 225 pounds per square foot. Test section flow angularity was found to be minimal with a generally random flow pattern. Corrections for survey rake induced in-plane flow were determined to be necessary; however, corrections for rake induced lift effects were not required.

Introduction

Wind tunnels, like any measurement instrument, require calibration in order to provide reliable and accurate information. A wind tunnel calibration involves determining the mean values and uniformity of various flow parameters in the tunnel test section. For a low-speed tunnel that operates at Mach numbers of 0.5 and below, the calibration typically involves determining the distribution of dynamic pressure, static pressure, total pressure, temperature, turbulence, and flow angularity. The calibration of tunnels that operate in the transonic and supersonic regions (Mach numbers from 0.8 to 5.0) is focused on determining the distribution of Mach number along the test section centerline. A good distribution of Mach number along the test section of a transonic tunnel is generally indicative of smooth flow (ref. 1). However, flow angularity and turbulence should still be determined for completeness. Wind tunnel calibrations are typically conducted on a regular basis to monitor flow conditions or after any changes or modifications have been made to the facility. In the case of the Langley Transonic Dynamics Tunnel (TDT), a calibration was conducted following a facility modification.

The TDT is a continuous-flow tunnel with a slotted test section and is capable of operation up to Mach 1.2 at stagnation pressures from near vacuum to atmospheric. The tunnel test section is 16 ft square with cropped corners and has a cross-sectional area of 248 ft^2. A unique feature of the TDT is that either air or heavy gas may be used as the test medium. In 1997 a modification to the TDT that involved changing the heavy gas test medium was completed. Until this modification, the heavy gas used at the TDT was Freon-12. The facility modification involved changing the test medium from Freon-12 to R-134a (ref. 2). As a result of this change in the tunnel test medium, it was decided to conduct a calibration of the TDT test section.

The calibration of the TDT test section involved the measurement of a number of parameters. Total and static pressure and temperature measurements were made throughout the tunnel to ensure the accuracy of calculated tunnel flow parameters -- for example, Mach number, dynamic pressure, and test medium density. Measurements of test section sidewall pressures (ref. 3) and boundary layer thickness were made along with the measurement of static pressures on the test section centerline. Measurements of flow angularity and turbulence across the tunnel section were made at one test section streamwise location. The calibration data were obtained in both air and R-134a at total pressures, dynamic pressures, and Mach numbers typical of operation in the TDT. The results of the turbulence study are presented in reference 4. The results presented in this report are for the flow angularity measurements made across the tunnel test section at one test section streamwise location. These flow angularity distribution data were taken in R-134a at dynamic pressures of 100 and 225 pounds per square foot at Mach numbers from 0.50 to 1.19.

Symbols

a	speed of sound, ft/sec
C_P	differential pressure coefficient
$C_{P_{align}}$	differential pressure coefficient due to probe alignment error
$C_{P_{AC}}$	probe differential pressure coefficient determined from orifices A and C, $C_{P_{AC}} = \frac{P_A - P_C}{P_E - P_{avg}}$
$C_{P_{BD}}$	probe differential pressure coefficient determined from orifices B and D, $C_{P_{BD}} = \frac{P_B - P_D}{P_E - P_{avg}}$
$C_{P_{\theta_{SR}}}$	slope of differential pressure coefficient versus survey rake pitch angle, per deg
M	Mach number
P_A	pseudo-static pressure measured by probe orifice A, psi
P_B	pseudo-static pressure measured by probe orifice B, psi
P_C	pseudo-static pressure measured by probe orifice C, psi
P_D	pseudo-static pressure measured by probe orifice D, psi
P_E	stagnation pressure measured by probe orifice E, psi
P_t	tunnel total pressure, psf
P_{avg}	Average probe pressure, $P_{avg} = (P_A + P_B + P_C + P_D)/4$, psi
q	dynamic pressure, psf
α	tunnel upflow angle, positive up, deg
$\alpha_{centerline_{horiz}}$	upflow angle measurement from survey rake centerline probe, deg
$\alpha_{induced}$	survey rake induced inplane flow angle, deg
α_{vert}	survey rake upflow angle measured in vertical orientation, deg
θ_{SR}	survey rake pitch angle, positive nose up, deg
θ_{SR_0}	survey rake pitch angle for zero upflow at probe tip, positive nose up, deg
β	tunnel sideflow angle, positive for flow to the right when viewed upstream, deg
β_{corr}	survey rake corrected sideflow angle component, deg
β_{meas}	survey rake uncorrected sideflow angle measurement, deg
$\Delta\beta_{horiz}$	survey rake sideflow angle correction, deg
σ	standard deviation

Abbreviations

psi	pounds per square inch
psf	pounds per square foot

Apparatus and Procedures

Wind Tunnel

The measurements documented in this report were made to assess the flow angularity distribution across the test section of the Langley Transonic Dynamics Tunnel (TDT) (figures 1 and 2). The TDT is a continuous flow tunnel capable of operating at Mach numbers up to 1.20 at pressures from near vacuum to atmospheric. Either air or R-134a may be used as test mediums. The TDT operating envelope is presented in figure 3 as a function of Mach number and dynamic pressure for the R-134a test medium. The use of a heavy gas, such as R-134a, as a test medium has advantages over air by simplifying aeroelastically-scaled model construction, reducing the time scale for model dynamics, and providing closer simulation of Froude number and Mach number while operating at higher Reynolds numbers.

The TDT test section is 16-ft square with cropped corners and has a cross-sectional area of 248 ft^2. Transonic flow is achieved by the use of three slots in both the test section ceiling and floor. These floor and ceiling slots provide an open area of 2.1 percent of the cross-sectional area to permit expansion of the flow. An additional 2.3 percent of open area is provided by slots in the test section sidewalls and serve to reduce the effects of model blockage. Ceiling and floor diffuser flaps spanning the width of the test section at the downstream end of the slots are used to control flow re-entry during transonic operation.

The TDT method of adjusting tunnel velocity involves controlling the fan drive motor rotational speed. Once the drive motor rotational speed limitation is reached, a set of pre-rotation vanes is used to vary the inflow to the fan and change the fan blade angles-of-attack, thereby changing the tunnel velocity. The effects of both the diffuser flaps and pre-rotation vanes were addressed during the flow angularity measurements.

Flow Survey Rake and Probes

The flow angularity measurements were accomplished by using five-hole pyramid-head probes mounted on a survey rake as shown in figures 4 through 6. The survey rake, as shown in figure 4, is mounted to a movable sting, which is in turn attached to the tunnel splitter plate located downstream of the test section. The movable sting is used to position the survey rake in both pitch and vertical translation. The survey rake spans 10.5 ft and provides for the streamwise mounting of 11 five-hole probes. One probe is mounted in the center of the rake and the remaining probes are mounted along the rake span, on either side of the rake centerline, at one-foot intervals. The probes are mounted in the survey rake such that the tips of the probes are placed at tunnel station 72, the typical streamwise location for aircraft models tested in the TDT. Each five-hole probe is mounted in the survey rake such that it can be rotated at 90-degree intervals, about the probe longitudinal axis, through a full 360 degrees. A spanwise cutout in the rake body (figure 5) provides volume for probe mounting hardware, instrumentation, and associated cabling. As shown in figure 6, each probe has four pseudo-static orifices, one on each face of the pyramidal tip, and a stagnation pressure orifice at the apex of the probe tip. The pseudo-static orifices are referred to in this manner because their orientation on the probe tip does not result in a purely static measurement. The pseudo-static orifices are designated as *A*, *B*, *C*, and *D*, and the stagnation orifice is designated as *E*. Measurement of the pressure differences between opposing pseudo-static orifices, i.e. *A* and *C* and *B* and *D*, allow the determination of orthogonal flow angles because the flow angularity is proportional to the pressure difference between opposing orifices.

Instrumentation

Instrumentation mounted in the rake body consisted of accelerometers for determining rake dynamic response and electronically scanned pressure (ESP) modules (ref. 5) for acquiring the five-hole probe pressure data. Four 16-port ESP modules were used to measure the five-hole probe

steady-state pressure data, each measuring differential pressure referenced to the tunnel plenum static pressure and selected to provide the best measurement accuracy for the test conditions. Three of the ESP modules measured probe pseudo-static pressures over a 2.5 psi range, and the remaining ESP module measured probe stagnation pressure over a 5 psi range. Pitch angle transducers were mounted on the sting and rake body to determine rake pitch angle.

Probe Calibration

To provide an accurate assessment of the flow angularity in the TDT test section the 5-hole probes were first calibrated. The method employed for this study is similar to that used in reference 6. The transonic flow characteristics of the TDT require that such calibrations be performed as a function of Mach number. However, because of the variable density capabilities of the TDT it is also necessary for the probe calibrations to be performed at various tunnel total pressures. Therefore, to provide a representative view of the flow angularity in the TDT throughout the operating range, a set of Mach and dynamic pressure combinations were chosen such that both the tunnel total pressure and the tunnel drive speed were varied. Probe calibrations were performed at each of the following nominal conditions: Mach numbers of 0.50, 0.70, 0.85, 0.90, 0.95, 1.00, 1.05, 1.10, and 1.19 and dynamic pressures of 100 psf and 225 psf for each Mach number.

Calibration data were acquired concurrently for all 11 probes with the rake in a vertical orientation. This procedure consisted of varying the sting pitch angle between -3° and +3° in 1° increments and recording the mean pressure for each orifice with the probes at a fixed roll orientation. The data acquisition procedure was repeated with the probes rolled in 90° increments until data had been acquired with each orifice in both an upright and inverted position. The resulting probe data were converted to differential pressure coefficients defined as:

$$C_{P_{AC}} = \frac{P_A - P_C}{P_E - P_{avg}}$$

$$C_{P_{BD}} = \frac{P_B - P_D}{P_E - P_{avg}}$$

where

$$P_{avg} = \frac{P_A + P_B + P_C + P_D}{4}.$$

These pressure coefficients relate the measured pressures to the local flow angle. Using this method a set of cross-plots were generated to calibrate the probes for flow angularity measurements while removing errors due to probe misalignment and local flow angle of the tunnel freestream. This cross-plot technique is shown conceptually in figure 7 and demonstrated in figure 8 with a representative set of data from the probe calibration.

Figure 7 shows the conceptual result obtained when calibrating a pressure probe for making upflow angle measurements. A similar technique is applied for the development of calibrations for sideflow angle measurements. For the upflow angle calibration, differential pressure coefficients, $C_{P_{AC}}$, are obtained with the probes in both an upright and inverted orientation and are then plotted as a function of survey rake pitch angle, θ_{SR}.

As indicated in figure 7(a), the results are typically linear for the range of rake pitch angles tested. The slope of each curve, $C_{P_{\theta_{SR}}}$, identifies the sensitivity of the differential pressure coefficient to the survey rake pitch angle. The intersection of the curves establishes the survey rake pitch angle required to obtain a zero upflow condition at the probe tip, θ_{SR_0}, and the differential pressure coefficient due to a physical probe alignment error, $C_{P_{align}}$. This information is then used to construct the final calibration curve for the probe in the upright orientation. The final calibration curve relates measured differential pressure coefficient, C_P, to the local upflow angle, α, as shown in figure 7(b). This curve is obtained by adjusting the original upright probe calibration curve (from figure 7(a)) by the survey rake pitch angle necessary to eliminate the

upflow, θ_{SR_0}. The final probe calibration curve then represents the measured differential pressure coefficient, C_P, as a function of local flow angularity, α, at a zero survey rake pitch angle ($\theta_{SR} = 0°$) and may be defined by the equation:

$$C_P = C_{P_{\theta_{SR}}} \alpha + C_{P_{align}}.$$

Then local flow angles may be determined directly from the differential pressure coefficients acquired during the measurement phase of the testing using:

$$\alpha = \frac{C_P - C_{P_{align}}}{C_{P_{\theta_{SR}}}}.$$

Figure 8 provides a representative set of probe calibration data with the linear fits indicated for the probe upright and inverted, and the intersection of the two curves that defines the survey rake pitch angle for zero upflow (θ_{SR_0}) and probe alignment error calibrations ($C_{P_{align}}$). Also shown are the residuals calculated for each of the linear fits and an indication of the 2σ (95%) confidence levels. The results shown are typical for most of the data set with regard to the quality of the linear fit and the statistical quality of the data.

Data Acquisition Considerations

Of primary concern for the TDT flow angularity calibration effort was the accurate acquisition of mean pressure data. This resulted in an extensive set of data acquired to address pressure settling times and appropriate data acquisition rates and duration. It was determined that it was necessary to allow a 5 minute settling time before data acquisition could commence when a new wind tunnel test condition, defined as a change in either Mach number or dynamic pressure, was established. It was also determined that the ESP sampling rate was not an important factor for the acquisition of mean pressure data. However, acquisition duration was concluded to be an important factor and a duration of 30 seconds was established for all flow angularity calibration testing. Figure 9 presents a representative result used for establishing this criteria. The figure shows the mean pressure for a single pseudo-static orifice as a function of data acquisition duration. As shown, the mean value of pressure is well established within 30 seconds. Other pressure measurements indicated similar behavior.

Of secondary concern for the TDT flow angularity measurement effort was a reasonable assessment of the data quality and accuracy. While some of this assessment relies upon the development of proper data acquisition techniques as discussed previously, it was determined that additional assessments should be made where possible to gain confidence in the entire test setup. As described below, these additional assessments included: a study of the local upflow angles identified during probe calibration; a statistical analysis of the probe calibration results; and an examination of the probe calibration repeatability.

Local Upflow Angles

As has been described, it was necessary to make incremental rotations of the probes during the calibration phase of the testing. These rotations included orientations in which each pseudo-static orifice was in either an upright or an inverted position. From these data the flow angularity calibration figures were generated (see figure 8). As a result of this procedure a set of calibration data was generated for orifices *A* and *C*, and for orifices *B* and *D*. In theory, although the sensitivity and probe angularity offset due to any probe misalignments may be different for these two pairs of probe orientations, the local upflow angle identified by the calibration technique should be the same for each orientation. Table 1 presents the results of the vertical plane flow angularity (upflow) identified by the calibration of orifices *A* and *C* (i.e., orifice *A* oriented "up"), and *B* and *D* (i.e., orifice *B* oriented "up"). The maximum angle difference of 0.25° was observed at a tunnel condition of M = 1.10 and q = 225 psf for the calibration data set.

Statistical Analysis of the Probe Calibration Results

As shown in figure 8, the residuals of each probe calibration fit have been calculated and a 2σ (95% confidence) boundary generated. Of the nearly 800 linear fits generated for the probe calibration data set only 26 contain any points that extend beyond the 2σ boundary. The standard deviation for most data fits resulted in a variation in flow angularity that is less than 0.05°, and the maximum standard deviation of any of the fits was determined to be 0.15°. Applying a 2σ boundary using the maximum standard deviation results in a 95% confidence interval of ±0.30°. Based on the results of the statistical analysis and the results presented in Table 1 which indicated errors of up to 0.25°, the error band for the entire probe calibration and flow angularity measurement data sets has been set to ±0.30°.

Probe Calibration Repeatability

Several Mach number and dynamic pressure combinations were selected to repeat the probe calibrations with orifices *A* and *B* in the upright position. The data that were acquired have been examined to assess the repeatability of the probe calibration and were found to fully support the previously stated error band of ±0.30°.

Results and Discussion

Initial Flow Angularity Maps

Flow angularity maps for a dynamic pressure of 100 psf are shown in figure 10. The data are presented in a vector format with 1 foot of test section dimension equivalent to 1 degree of flow angularity. The plots show the outline of the TDT test section, including flow expansion slot placement, and the relative location of the flow angularity measurements. The data are presented looking upstream. That is, the right wing of an aircraft model mounted on the tunnel centerline will experience the flow conditions shown on the right side of the flow maps.

All data shown were acquired with the flow angularity rake placed in a horizontal orientation and the probes installed with orifice *A* upright. Prior to data acquisition the vertical position of the rake was set by traversing the TDT sting apparatus and the pressure measurement systems were permitted time to settle. Then, data were acquired for 30 seconds and resolved into horizontal and vertical flow components using the calibration parameters determined previously for each probe. The rake was then repositioned by traversing the sting and new data were acquired. Rake repositioning and data acquisition were repeated until flow angularity measurements had been made at 11 vertical locations, extending in 1 foot increments, from 5 feet below to 5 feet above the test section centerline. At each tunnel condition, three sets of data were acquired for the centerline position and serve as a check on the measurement repeatability.

Figure 10 presents test section flow angularity maps at a dynamic pressure of 100 psf for Mach numbers ranging from 0.50 to 1.19. The flow map presented in figure 10(b) is incomplete due to data acquisition difficulties. A study of the flow angularity maps presented in figure 10 reveals flow which is generally horizontal and directed toward the test section walls, behavior that is not considered to be a realistic flow condition. Additionally, a review of the flow angularity data generated during probe calibration, with the survey rake in the vertical orientation, indicates a flow trend towards the test section ceiling and floor. As shown in figure 11, this trend of flow towards the ceiling and floor with the survey rake oriented vertically is of approximately the same magnitude for both q = 100 psf and q = 225 psf. Therefore, the dominant flow trends with the survey rake in the measurement (horizontal) and probe calibration (vertical) orientations are considered to be due to a flow induced in the plane of the survey rake. Because this flow is believed to be induced solely by the presence of the survey rake, a method was sought to eliminate it from the measurement set. The subsequent section will describe the measurement correction procedure used.

Corrected Flow Angularity Maps

Figures 12 and 13 present the corrected flow angularity maps for q = 100 psf and q = 225 psf respectively for Mach numbers ranging from 0.50 to 1.19. As discussed for figure 10(b), the maps presented in figure 12(b) and 13(i) are incomplete due to data acquisition difficulties. The inplane flow corrections were made using the assumptions that 1) the spanwise flow along the rake plane does not change when the rake is yawed slightly with respect to the flow, and 2) the flow perpendicular to the rake plane is not significantly affected by the presence of the rake body at small angles-of-attack. The first assumption permits the acceptance of the probe calibration angle-of-attack sensitivity as a valid value. This is because the probes are calibrated with the rake installed in a vertical orientation. If the probe angle-of-attack sensitivity was affected significantly by yawed flow across the rake body, then all flow angularity measurements made using the probe calibrations as described previously would be invalid. The second assumption permits the acceptance of vertical flow angularity measurements made with the rake in a horizontal orientation. Therefore, all α (upflow) measurements made during the flow angularity measurement phase may be considered to be valid. It is only the β (sideflow) measurements that require correction.

The procedure used to remove the inplane flow effects from the final data is:

1) Measure the upflow angle (α_{vert}) at each probe location along the survey rake for each tunnel condition with the rake in the vertical (calibration) orientation.

2) Measure the upflow angle at the centerline probe ($\alpha_{centerline_{horiz}}$) with the survey rake in the horizontal (measurement) orientation. Data are required for rake heights of –5, -4, -3, -2, -1, 0, +1, +2, +3, +4, and +5 feet, referenced to test section centerline, so that the measurements correspond to the same spatial locations as measured by the 11 probes in step 1.

3) Using the equation:

$$\alpha_{induced} = \alpha_{centerline_{horiz}} - \alpha_{vert}$$

calculate the induced inplane flow effects, $\alpha_{induced}$, due to the survey rake body.

4) Make the assumption that a sideflow angle correction, $\Delta\beta_{horiz}$, with the survey rake in the horizontal orientation is the same as the induced inplane flow effects due to the survey rake body with the survey rake in the vertical orientation, $\alpha_{induced}$. Therefore, the induced inplane flow angle for each probe may be used as a sideflow correction:

$$\Delta\beta_{horiz} = \alpha_{induced}.$$

5) Calculate the corrected sideflow angle, β_{corr}, for each measurement location using the individual probe sideflow correction, $\Delta\beta_{horiz}$,

$$\beta_{corr} = \beta_{meas} - \Delta\beta_{horiz}$$

where β_{meas} is the uncorrected measurement of sideflow.

Examination of figures 12 and 13, for which sideflow corrections have been applied, shows that the sideflow previously attributed to the rake body (in figure 10) is no longer evident. It is also noted that, with the exception of the highest Mach number condition (M = 1.19), larger sideflow components were removed at the higher Mach numbers. This is further supported by the results presented in figure 11 in which the upflow with the survey rake in the vertical (calibration) orientation is presented for each Mach number condition tested.

Figure 12 presents the corrected flow angularity measurements for a dynamic pressure of 100 psf for Mach numbers ranging from 0.50 to 1.19. The results show that the flow angularity is more or less random with generally small values (i.e., $|\alpha| \leq 0.5°$ and $|\beta| \leq 0.50°$ for most cases). The small, random flow angularity values would generally support a conclusion that little flow angularity exists in the test section,

particularly considering the previously developed measurement accuracy assessment of ±0.30°. Also noted in figure 12 is that no significant differences are observed between the subsonic and transonic flow angularity measurements indicating a generally consistent flow throughout the speed range. A notable exception to this is shown in the flow pattern for M = 1.10 (figure 12(h)) in which the flow appears to be directed toward the test section centerline. A further review of the data acquired and the corrections applied revealed no explanation for this phenomenon.

Figure 13 presents the corrected flow angularity measurements for a dynamic pressure of 225 psf for Mach numbers ranging from 0.50 to 1.19. As with the results presented for q = 100 psf, the measurements at q = 225 psf indicate a relatively random flow pattern. It is noted that the flow vectors for the lower speed range (M = 0.50 and 0.70) are generally larger than those for the same speed range at q = 100 psf. Otherwise, similar flow angularity trends exist for both dynamic pressures including the trend of the centerline-directed flow pattern at M = 1.10.

In summary, with the exception of the flow at M = 1.10, no consistent test section flow pattern is noted for the conditions at which data were acquired. Considering the stated accuracy of the measurements (±0.30°) and the generally random flow pattern shown in figures 12 and 13, the flow angularity in the TDT test section is considered to be minimal based on the results of this investigation.

Effect of Pre-Rotation Vanes and Diffuser Flaps on Flow Angularity

As discussed previously, the TDT uses pre-rotation vanes to assist in the control of tunnel velocity, and test section ceiling and floor diffuser flaps to control flow re-entry during transonic operation. Data were acquired to assess the effects of both the pre-rotation vane and the diffuser flap settings on test section flow angularity at the conditions shown in Table 2. The data to assess the impact of the pre-rotation vanes were acquired for three vane angular settings at each of the tunnel conditions indicated in Table 2. The data to assess the impact of the diffuser flaps were acquired using established flap settings required to achieve transonic flow, as well as deviations from these settings.

In general, the pre-rotation vane and the diffuser flap studies showed that neither of the systems had a pronounced impact on the flow angularity evident in the test section. The pre-rotation vane assessment showed that, in general, variations in the test section flow angularity were limited to 0.10°. The greatest changes in flow angularity due to variations in pre-rotation vane angles were determined to be at the lowest Mach number tested, M = 0.50. These changes, however, were sparse and limited to 0.30°, the previously stated error band limit for the data set. This indicates that the changes in flow angularity are relatively insignificant and are independent of the pre-rotation vane angle settings. A similar set of results were obtained for the diffuser flap setting study. The changes in flow angle due to variation in the diffuser flap setting were typically limited to an even smaller range than that obtained during the pre-rotation vane angle study. Therefore, as for the pre-rotation vane settings, the test section flow angularity is considered to be independent of diffuser flap settings.

Survey Rake Lift Effects

Previous investigations in other wind tunnels have indicated a potential for contamination of flow angularity measurements due to rake lift effects (refs. 6 and 7). Therefore, for the current study additional flow angularity measurements were made with the survey rake in the horizontal orientation while the pitch was varied from -3° to +3° in 1° increments. These data were limited to M = 0.70 and M = 1.10 at dynamic pressures of 100 psf and 225 psf to provide an indication of the rake lift effects for the current data set. Figure 14 presents the upflow as a function of survey rake pitch for M = 0.70 and M = 1.10 at q = 100 psf. As shown in figure 14(a), none of the slopes are 1.0 indicating that rake lift effects do have some impact on the measured upflow for the subsonic condition (M = 0.70). Figure 14(b) shows that the upflow slopes at M = 1.10 are

approximately equal to 1.0 indicating minimal lift effect. An inspection of the sideflow component, figures 15(a) and 15(b), shows nonzero slopes indicating a small effect of rake lift on sideflow at M = 0.70 and 1.10. Results similar to those presented in figures 14 and 15 were also obtained at q = 225 psf at both Mach numbers. The calculated slopes for the upflow are presented in figure 16 as a function of spanwise measurement station and indicates a typical lift distribution across the survey rake span at the subsonic speed (M = 0.70). Figure 16 also shows that there is minimal effect of rake lift at M = 1.10, as anticipated due to a lack of upflow in front of the rake body at this transonic condition.

Results of this investigation indicated that applying upflow corrections due to rake lift effects would decrease the upflow components by up to 0.25°. Sideflow corrections would be limited for all cases to ±0.10°. For all conditions examined, the lift corrections for either upflow or sideflow have been shown to be less than the stated accuracy of the data set (±0.30°). The lift effects, therefore, are not considered to be of great significance because their application would not alter the basic conclusion that the flow angularity in the TDT test section is minimal. Therefore, the lift corrections were not applied to any of the data presented herein.

Conclusions

An investigation has been conducted in the Langley Transonic Dynamics Tunnel (TDT) to measure the test section flow angularity at station 72, the typical streamwise location for models tested in the TDT. Flow measurements were made in a 10-ft square grid centered about the test section centerline. Measurements were made for 9 Mach numbers ranging from M = 0.50 to M = 1.19 at dynamic pressures of 100 psf and 225 psf. Based on the results obtained and presented herein, the following conclusions have been reached:

1. The accuracy of the acquired flow angularity data set is considered to be ±0.30°.

2. Corrections for survey rake induced in-plane flow were determined to be necessary.

3. Tunnel pre-rotation vane and test section diffuser flap settings were found to have minimal effect on test section flow angularity.

4. Corrections for survey rake induced lift effects were found to be less than the stated accuracy of the data set and, therefore, not applied.

5. The measured test section flow pattern is generally random with the exception of the flow at M = 1.10, in which the flow is directed towards the test section centerline.

6. Flow angularity in the test section is minimal.

References

1. Pope, Alan: “Wind-Tunnel Testing”, 2nd. Edition, John Wiley & Sons, Inc., 1964.

2. Corliss, J.M.; and Cole, S.R.: Heavy Gas Conversion of the NASA Langley Transonic Dynamics Tunnel. 20th AIAA Advanced Measurement and Ground Testing Technology Conference, June 15 – 18, 1998, Albuquerque, NM (AIAA Paper 98-2710).

3. Florance, James R.; and Rivera, Jose A., Jr.: Sidewall Mach Number Distributions for the NASA Langley Transonic Dynamics Tunnel. NASA TM-2001-211019, June 2001.

4. Wieseman, Carol D.; and Sleeper, Robert K.: Measurements of Flow Turbulence in the NASA Langley Transonic Dynamics Tunnel. NASA TM 2005-213529, February 2005.

5. System 8400 Users Manual, 4.0 Version; Pressure Systems, Inc., Hampton, Va., March 1996.

6. Yetter, J.A., and Abeyounis, W.K.: 16-Foot Transonic Tunnel Test Section Flow Feld Survey. NASA TM 109157, December 1994.

7. Smith, L., and Adcock, J.: Effect of Reynolds Number and Mach Number On Flow Angularity Probe Sensitivity. NASA TM 87750, September 1986.

Table 1. Vertical Plane Flow Angularity (Upflow) as Determined by Probe Calibration, deg

(a) M = 0.50, q = 100 psf

Probe Number	Probe Orientation		Difference |(A/C) - (B/D)|
	A/C vertical	B/D vertical	
1	-0.20	-0.22	0.02
2	-0.12	-0.11	0.01
3	-0.28	-0.13	0.15
4	0.06	-0.10	0.16
5	-0.03	0.11	0.14
6	-0.40	-0.46	0.06
7	-0.34	-0.27	0.07
8	-0.17	-0.19	0.02
9	-0.11	-0.18	0.07
10	-0.23	-0.06	0.17
11	-0.47	-0.36	0.11

(b) M = 0.70, q = 100 psf

Probe Number	Probe Orientation		Difference |(A/C) - (B/D)|
	A/C vertical	B/D vertical	
1	0.24	0.27	0.03
2	-0.03	0.03	0.06
3	-0.21	-0.20	0.01
4	-0.04	-0.12	0.08
5	-0.03	-0.02	0.01
6	-0.35	-0.37	0.02
7	-0.31	-0.27	0.04
8	-0.14	-0.29	0.15
9	-0.17	-0.26	0.09
10	-0.42	-0.26	0.16
11	-0.54	-0.45	0.09

(c) M = 0.85, q = 100 psf

Probe Number	Probe Orientation		Difference |(A/C) - (B/D)|
	A/C vertical	B/D vertical	
1	0.70	0.74	0.04
2	0.41	0.45	0.04
3	0.02	0.01	0.01
4	-0.01	-0.09	0.08
5	-0.06	-0.01	0.05
6	-0.34	-0.35	0.01
7	-0.31	-0.27	0.04
8	-0.21	-0.34	0.13
9	-0.39	-0.45	0.06
10	-0.71	-0.63	0.08
11	-0.89	-0.86	0.03

(d) M = 0.90, q = 100 psf

Probe Number	Probe Orientation		Difference |(A/C) – (B/D)|
	A/C vertical	B/D vertical	
1	0.95	1.01	0.06
2	0.63	0.68	0.05
3	0.19	0.18	0.01
4	0.11	0.01	0.10
5	0.00	0.04	0.04
6	-0.29	-0.32	0.03
7	-0.35	-0.31	0.04
8	-0.31	-0.46	0.15
9	-0.54	-0.61	0.07
10	-0.91	-0.89	0.02
11	-1.16	-1.17	0.01

(e) M = 0.95, q = 100 psf

Probe Number	Probe Orientation		Difference |(A/C) – (B/D)|
	A/C vertical	B/D vertical	
1	1.29	1.26	0.03
2	0.90	0.91	0.01
3	0.37	0.37	0.00
4	0.23	0.13	0.10
5	0.05	0.09	0.04
6	-0.29	-0.32	0.03
7	-0.40	-0.36	0.04
8	-0.42	-0.56	0.14
9	-0.74	-0.78	0.04
10	-1.19	-1.12	0.07
11	-1.48	-1.43	0.05

(f) M = 1.00, q = 100 psf

Probe Number	Probe Orientation		Difference |(A/C) – (B/D)|
	A/C vertical	B/D vertical	
1	1.50	1.48	0.02
2	1.10	1.10	0.00
3	0.54	0.52	0.02
4	0.38	0.24	0.14
5	0.15	0.13	0.02
6	-0.24	-0.30	0.06
7	-0.37	-0.43	0.06
8	-0.49	-0.65	0.16
9	-0.87	-0.95	0.08
10	-1.30	-1.29	0.01
11	-1.65	-1.64	0.01

Table 1. Continued.

(g) M = 1.05, q = 100 psf

Probe Number	Probe Orientation		Difference |(A/C – (B/D)|
	A/C vertical	B/D vertical	
1	1.57	1.55	0.02
2	1.16	1.16	0.00
3	0.57	0.58	0.01
4	0.35	0.28	0.07
5	0.11	0.17	0.06
6	-0.26	-0.29	0.03
7	-0.42	-0.43	0.01
8	-0.55	-0.66	0.11
9	-0.93	-0.98	0.05
10	-1.39	-1.33	0.06
11	-1.73	-1.67	0.06

(h) M = 1.10, q = 100 psf

Probe Number	Probe Orientation		Difference |(A/C) – (B/D)|
	A/C vertical	B/D vertical	
1	1.35	1.36	0.01
2	1.06	1.06	0.00
3	0.51	0.52	0.01
4	0.33	0.24	0.09
5	0.12	0.15	0.03
6	-0.25	-0.29	0.04
7	-0.42	-0.43	0.01
8	-0.51	-0.63	0.12
9	-0.85	-0.92	0.07
10	-1.25	-1.19	0.06
11	-1.44	-1.41	0.03

(i) M = 1.19, q = 100 psf

Probe Number	Probe Orientation		Difference |(A/C) – (B/D)|
	A/C vertical	B/D vertical	
1	-0.23	-0.23	0.00
2	0.01	0.01	0.00
3	-0.27	-0.22	0.05
4	-0.16	-0.25	0.09
5	-0.09	-0.07	0.02
6	-0.24	-0.26	0.02
7	-0.26	-0.30	0.04
8	-0.02	-0.14	0.12
9	-0.04	-0.19	0.15
10	-0.08	-0.03	0.05
11	-0.06	-0.08	0.02

(j) M = 0.50, q = 225 psf

Probe Number	Probe Orientation		Difference |(A/C) – (B/D)|
	A/C vertical	B/D vertical	
1	-0.05	-0.03	0.02
2	-0.23	-0.24	0.01
3	-0.06	-0.09	0.03
4	-0.03	-0.12	0.09
5	-0.19	-0.05	0.14
6	-0.33	-0.45	0.12
7	-0.29	-0.27	0.02
8	-0.13	-0.23	0.10
9	-0.10	-0.15	0.05
10	-0.23	-0.24	0.01
11	-0.47	-0.34	0.13

(k) M = 0.70, q = 225 psf

Probe Number	Probe Orientation		Difference |(A/C) – (B/D)|
	A/C vertical	B/D vertical	
1	-0.01	-0.04	0.03
2	-0.07	-0.12	0.05
3	-0.06	-0.06	0.00
4	0.11	-0.05	0.16
5	-0.13	0.01	0.14
6	-0.37	-0.39	0.02
7	-0.32	-0.27	0.05
8	-0.24	-0.16	0.08
9	-0.10	-0.20	0.10
10	-0.37	-0.30	0.07
11	-0.58	-0.56	0.02

(l) M = 0.85, q = 225 psf

Probe Number	Probe Orientation		Difference |(A/C) – (B/D)|
	A/C vertical	B/D vertical	
1	0.49	0.53	0.04
2	0.28	0.33	0.05
3	0.02	0.11	0.09
4	0.12	0.02	0.10
5	-0.07	0.00	0.07
6	-0.34	-0.37	0.03
7	-0.29	-0.18	0.11
8	-0.13	-0.18	0.05
9	-0.29	-0.35	0.06
10	-0.70	-0.58	0.12
11	-0.97	-0.90	0.07

Table 1. Concluded.

(m) M = 0.90, q = 225 psf

Probe Number	Probe Orientation		Difference |(A/C) – (B/D)|
	A/C vertical	B/D vertical	
1	0.79	0.85	0.06
2	0.53	0.55	0.02
3	0.24	0.29	0.05
4	0.23	0.12	0.11
5	0.13	0.03	0.10
6	-0.39	-0.31	0.08
7	-0.31	-0.28	0.03
8	-0.32	-0.27	0.05
9	-0.50	-0.45	0.05
10	-0.91	-0.75	0.16
11	-1.23	-1.18	0.05

(n) M = 0.95, q = 225 psf

Probe Number	Probe Orientation		Difference |(A/C) – (B/D)|
	A/C vertical	B/D vertical	
1	1.08	1.12	0.04
2	0.82	0.82	0.00
3	0.39	0.48	0.09
4	0.34	0.28	0.06
5	0.06	0.12	0.06
6	-0.32	-0.26	0.06
7	-0.32	-0.35	0.03
8	-0.47	-0.51	0.04
9	-0.71	-0.69	0.02
10	-1.19	-0.99	0.20
11	-1.54	-1.47	0.07

(o) M = 1.00, q = 225 psf

Probe Number	Probe Orientation		Difference |(A/C) – (B/D)|
	A/C vertical	B/D vertical	
1	1.33	1.37	0.04
2	1.10	1.04	0.06
3	0.57	0.63	0.06
4	0.43	0.35	0.08
5	0.04	0.17	0.13
6	-0.28	-0.28	0.00
7	-0.33	-0.35	0.02
8	-0.47	-0.60	0.13
9	-0.77	-0.81	0.04
10	-1.32	-1.08	0.24
11	-1.73	-1.65	0.08

(p) M = 1.05, q = 225 psf

Probe Number	Probe Orientation		Difference |(A/C) – (B/D)|
	A/C vertical	B/D vertical	
1	1.36	1.46	0.10
2	1.01	1.09	0.08
3	0.57	0.65	0.08
4	0.38	0.31	0.07
5	0.07	0.18	0.11
6	-0.31	-0.39	0.08
7	-0.33	-0.36	0.03
8	-0.63	-0.53	0.10
9	-0.88	-0.83	0.05
10	-1.35	-1.11	0.24
11	-1.78	-1.68	0.10

(q) M= 1.10, q = 225 psf

Probe Number	Probe Orientation		Difference |(A/C) – (B/D)|
	A/C vertical	B/D vertical	
1	1.17	1.27	0.10
2	0.90	1.01	0.11
3	0.53	0.61	0.08
4	0.36	0.28	0.08
5	0.07	0.17	0.10
6	-0.30	-0.26	0.04
7	-0.36	-0.34	0.02
8	-0.50	-0.47	0.03
9	-0.83	-0.77	0.06
10	-1.23	-0.98	0.25
11	-1.53	-1.40	0.13

(r) M = 1.19, q = 225 psf

Probe Number	Probe Orientation		Difference |(A/C) – (B/D)|
	A/C vertical	B/D vertical	
1	-0.25	-0.17	0.08
2	-0.16	-0.20	0.04
3	-0.18	-0.07	0.11
4	-0.18	-0.31	0.13
5	-0.18	-0.24	0.06
6	-0.27	-0.35	0.08
7	-0.10	-0.11	0.01
8	-0.01	-0.04	0.03
9	-0.13	-0.25	0.12
10	-0.07	0.13	0.20
11	-0.15	-0.14	0.01

Table 2. Test Conditions for Assessment of Diffuser Flap and Pre-rotation Vane Effect on Test Section Flow Angularity

Diffuser Flaps			Pre-rotation Vanes	
M	q = 100	q = 225	q = 100	q = 225
0.50			X	X
0.70				
0.85	X	X		
0.90			X	X
0.95	X	X		
1.00			X	X
1.05	X	X		
1.10				
1.19				

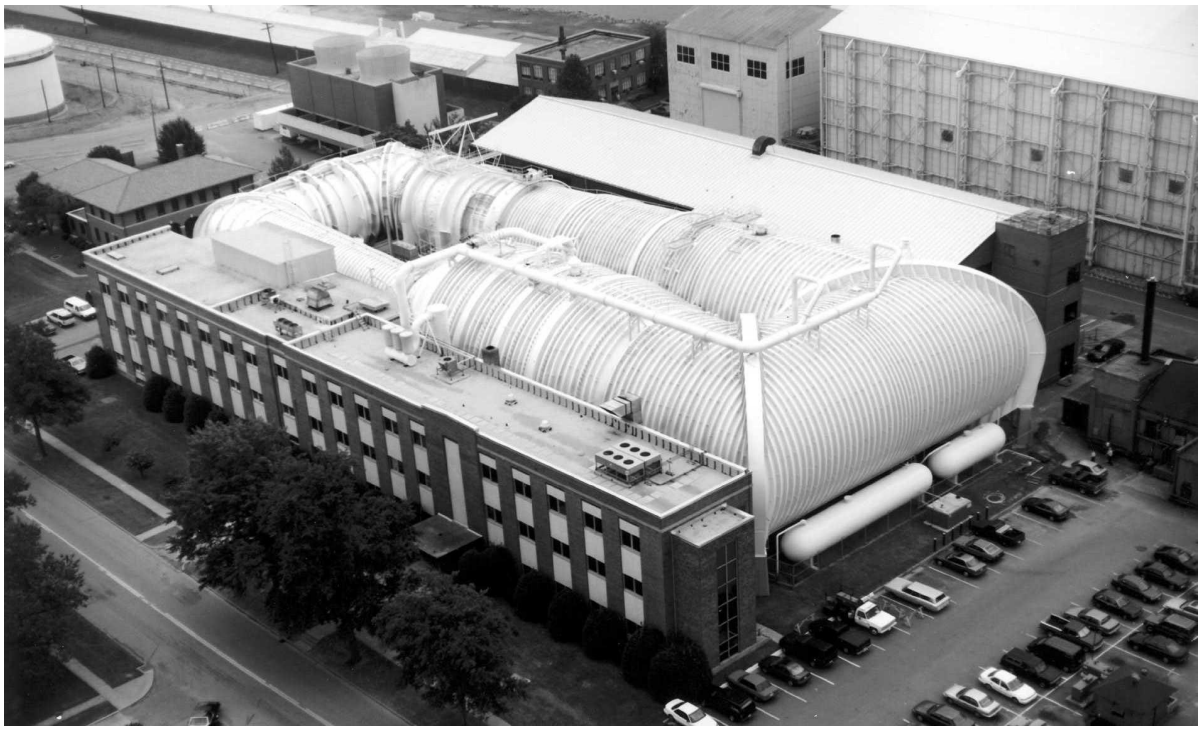

Figure 1. Langley Transonic Dynamics Tunnel (TDT).

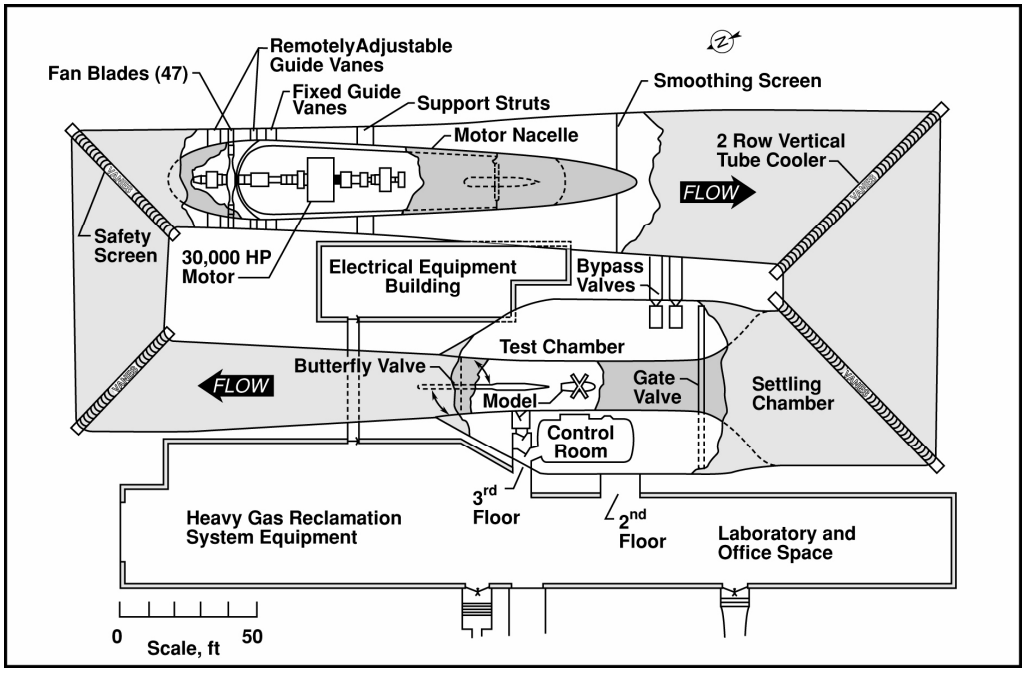

(a) Tunnel planform

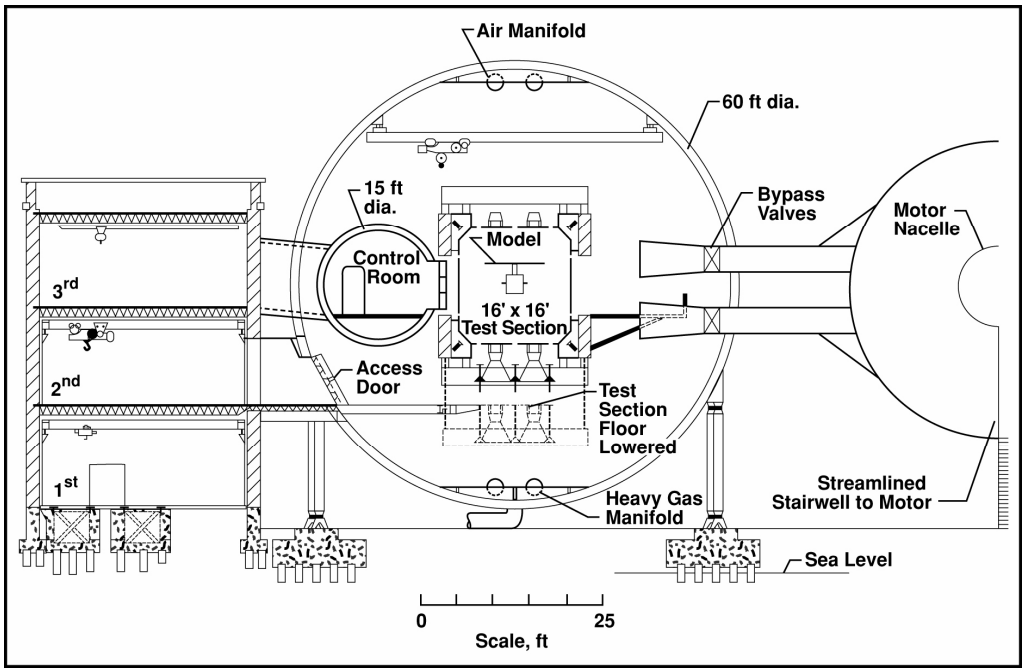

(b) Tunnel cross-section

Figure 2. General arrangement of TDT.

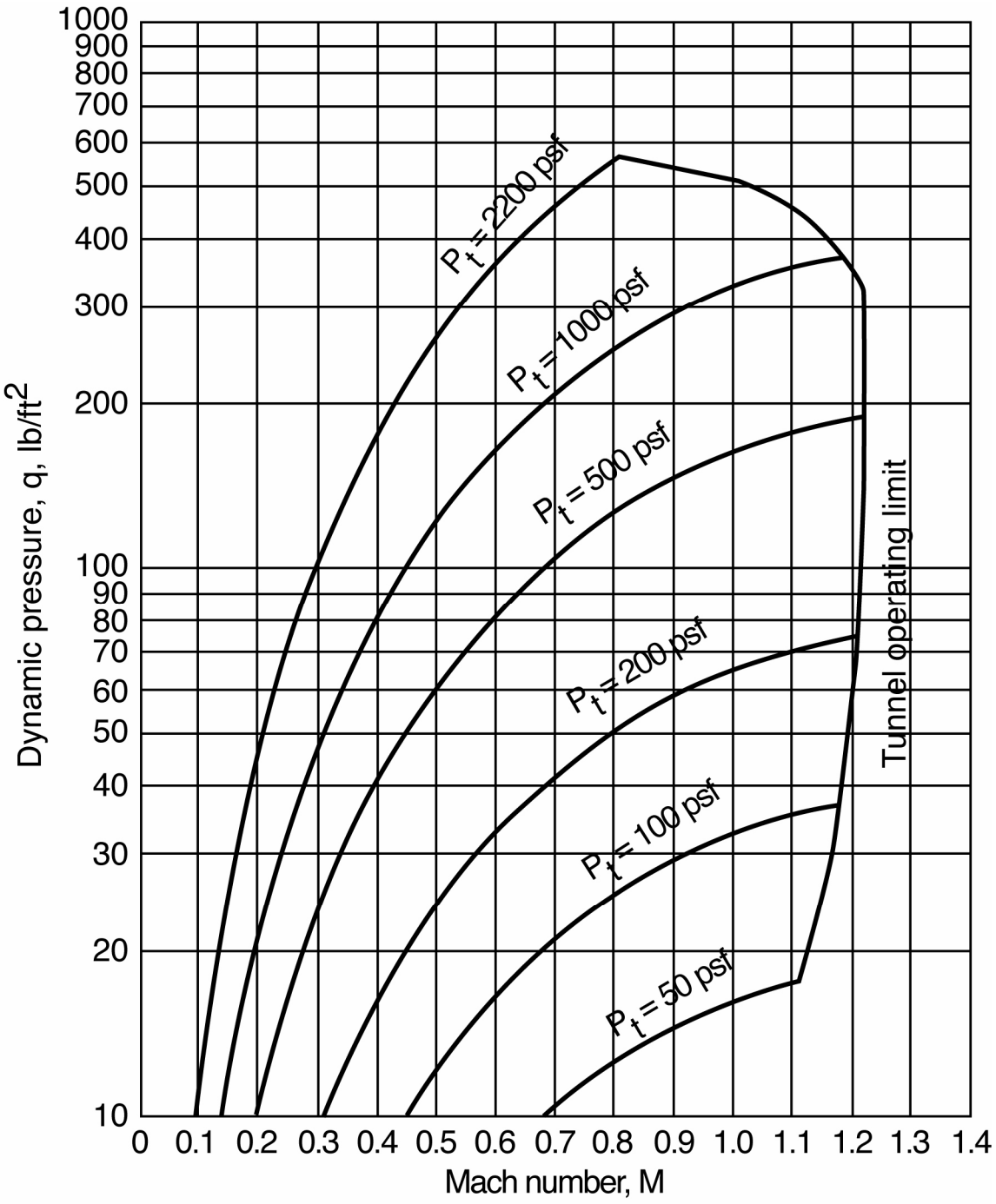

Figure 3. TDT R134a operating envelope.

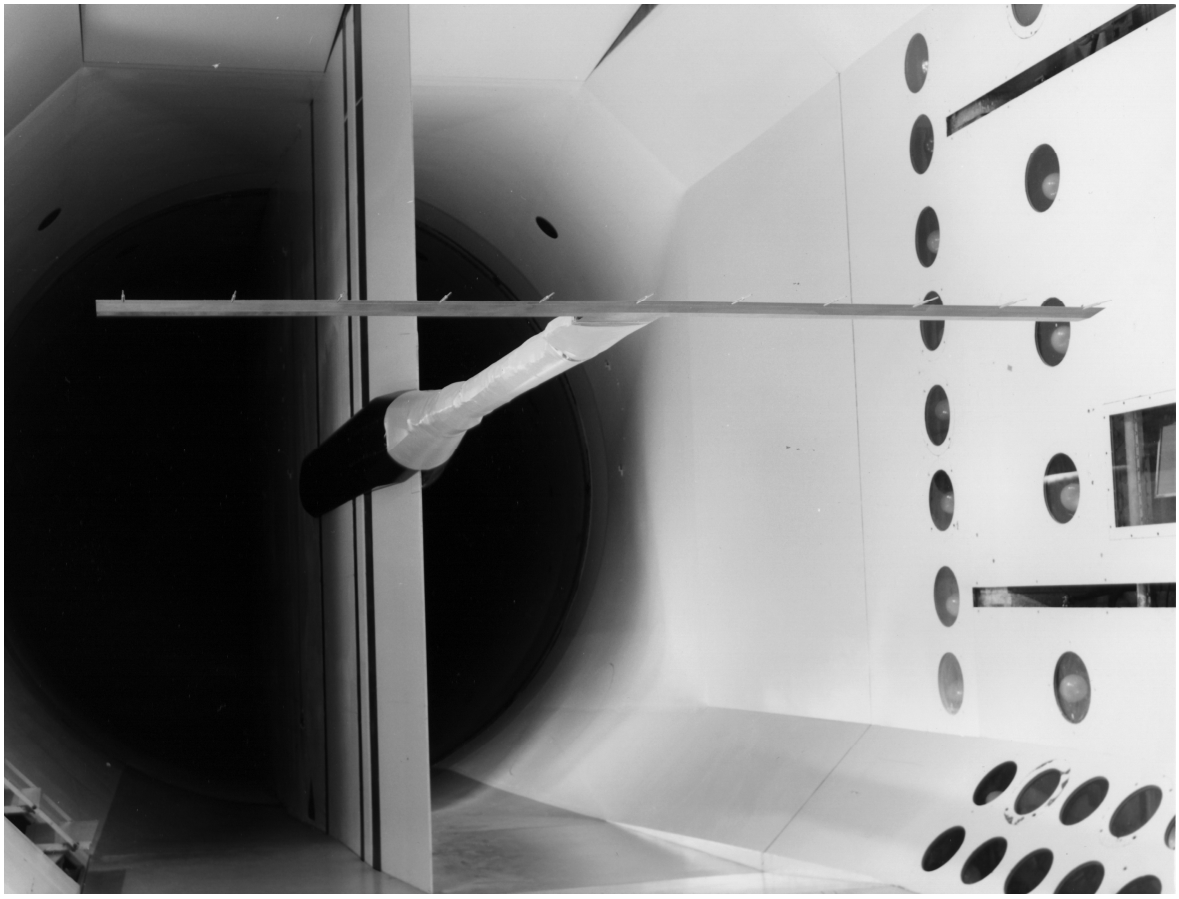

(a) Survey rake and 5-hole probes installed in TDT.

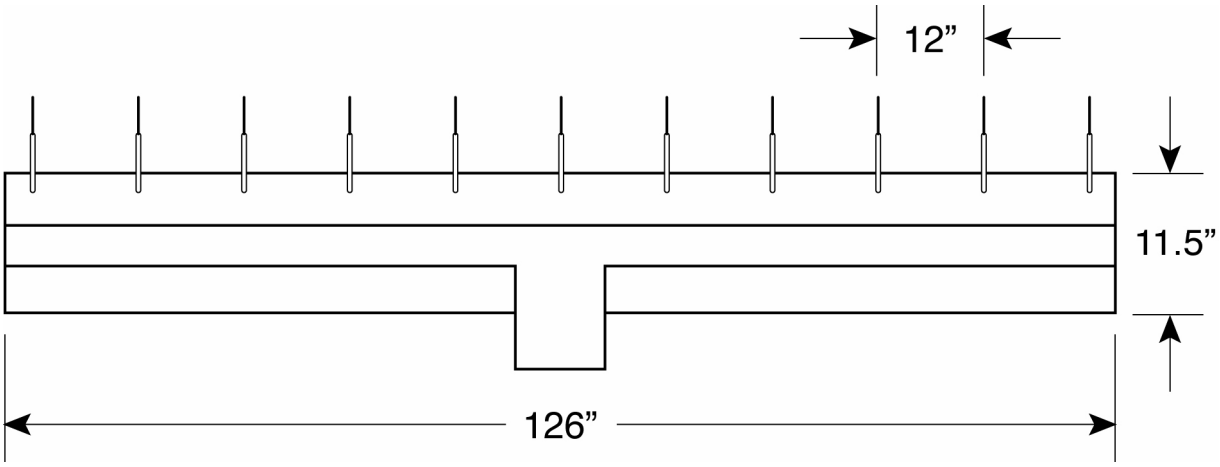

(b) Survey rake planform view

Figure 4. Survey rake.

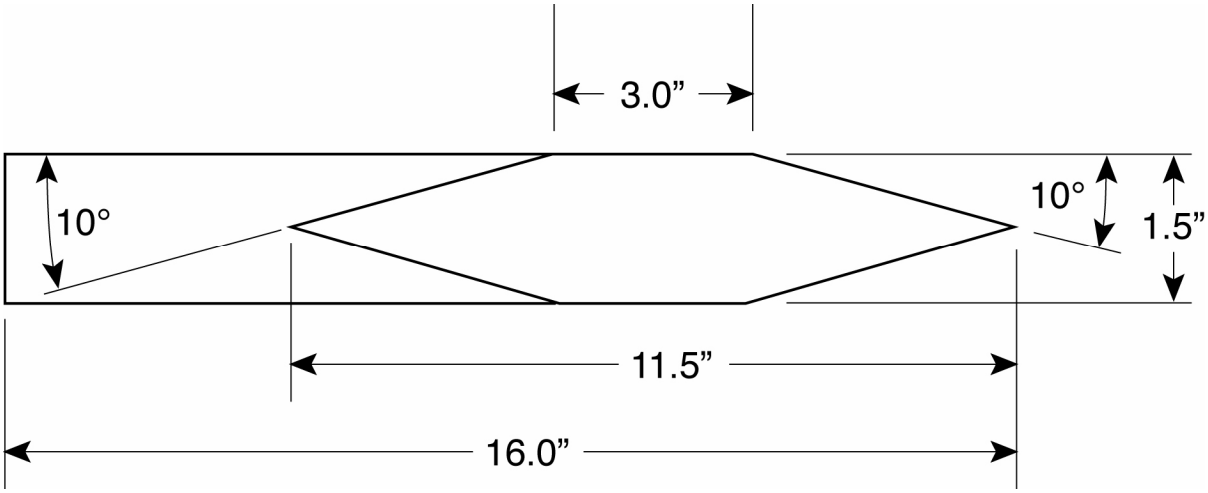

(c) Survey rake end view looking right to left along planform

Figure 4. Concluded.

Figure 5. Survey rake with instrumentation hatch removed.

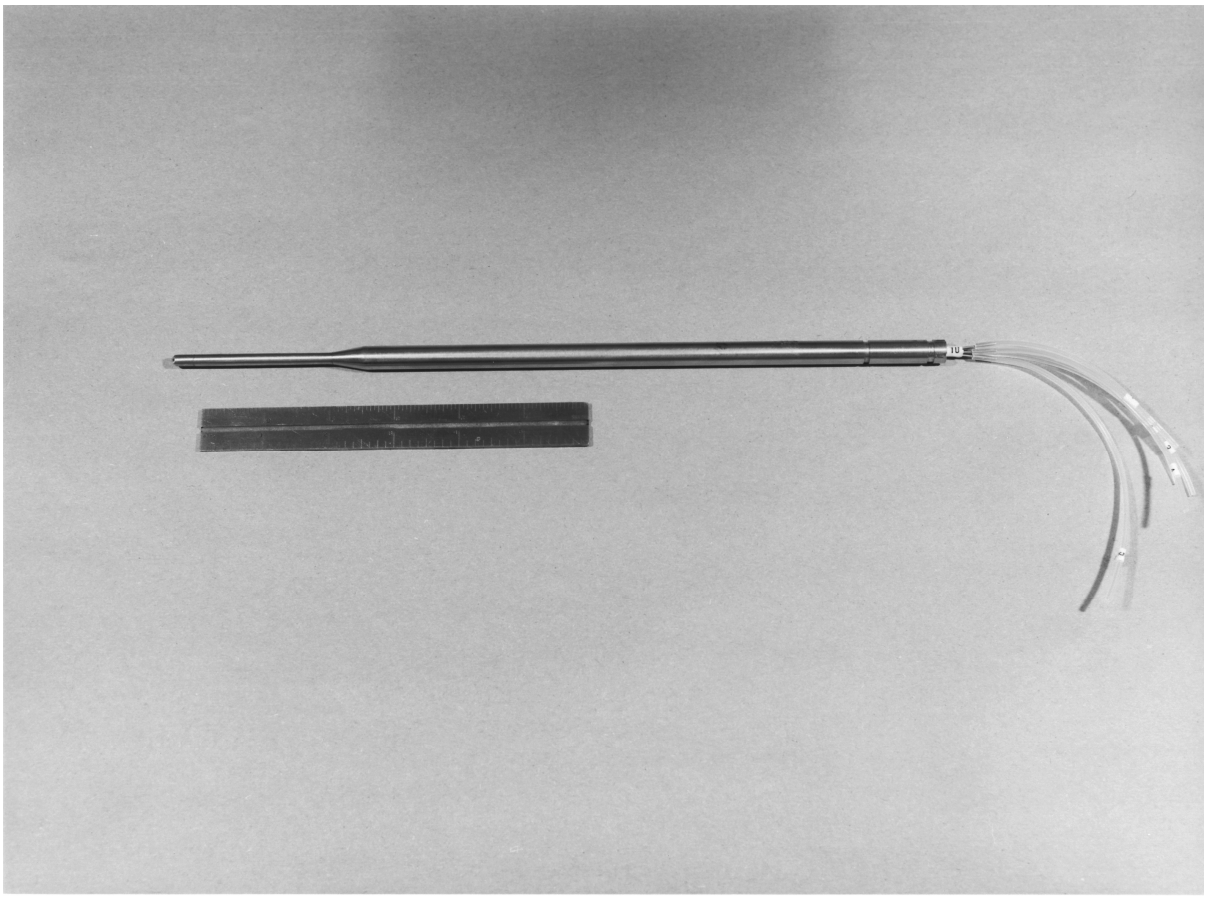

(a) Five-hole probe and tubing

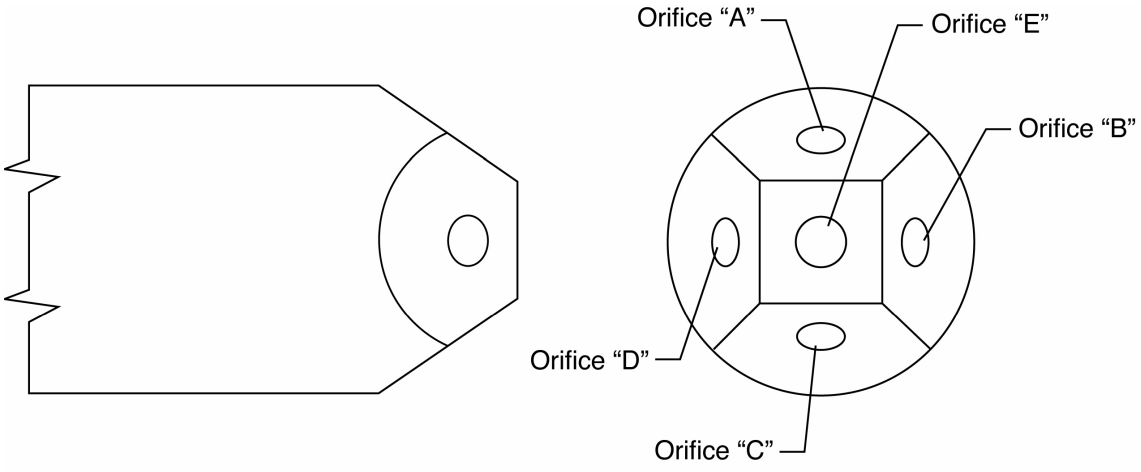

(b) Five-hole probe tip

Figure 6. Five-hole probe.

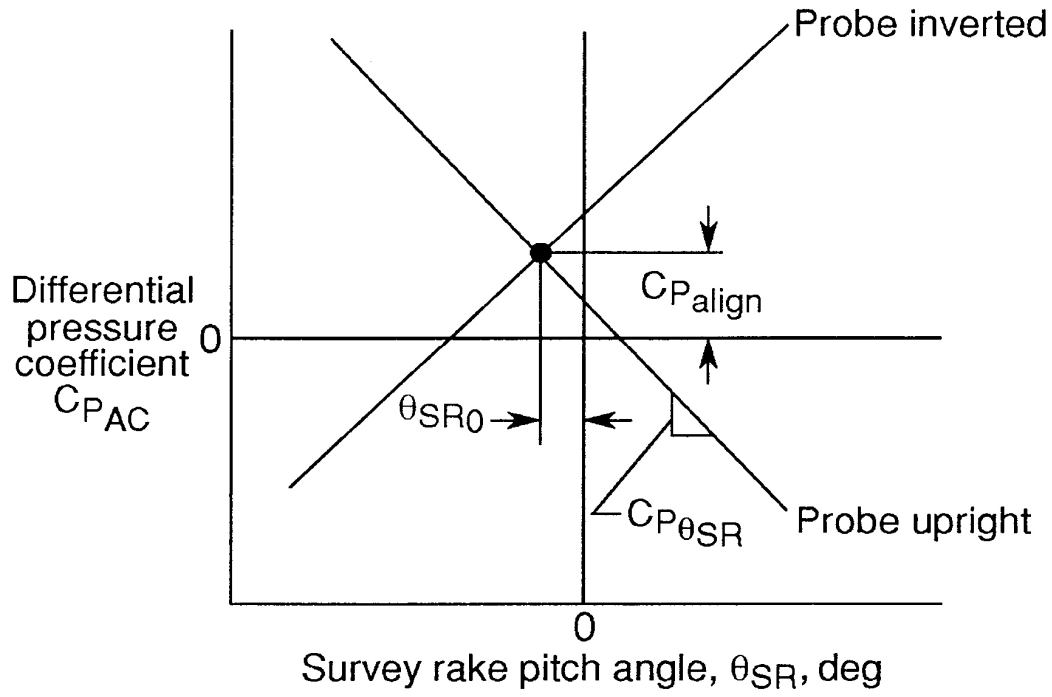

(a) Upright probe calibration curve

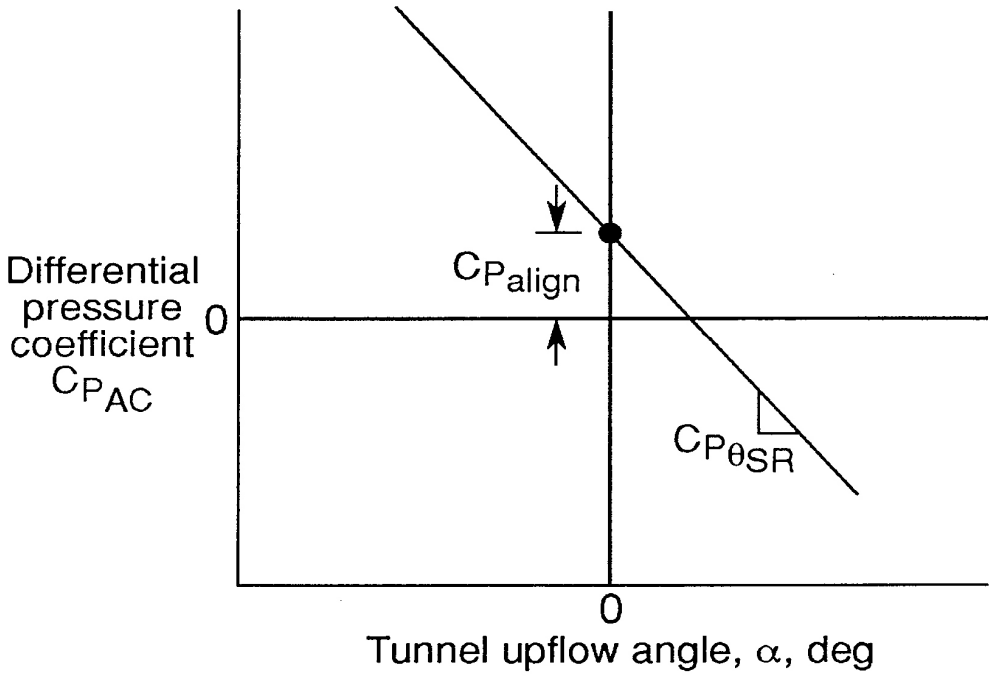

(b) Final probe calibration curve

Figure 7. Conceptual five-hole probe calibration curves.

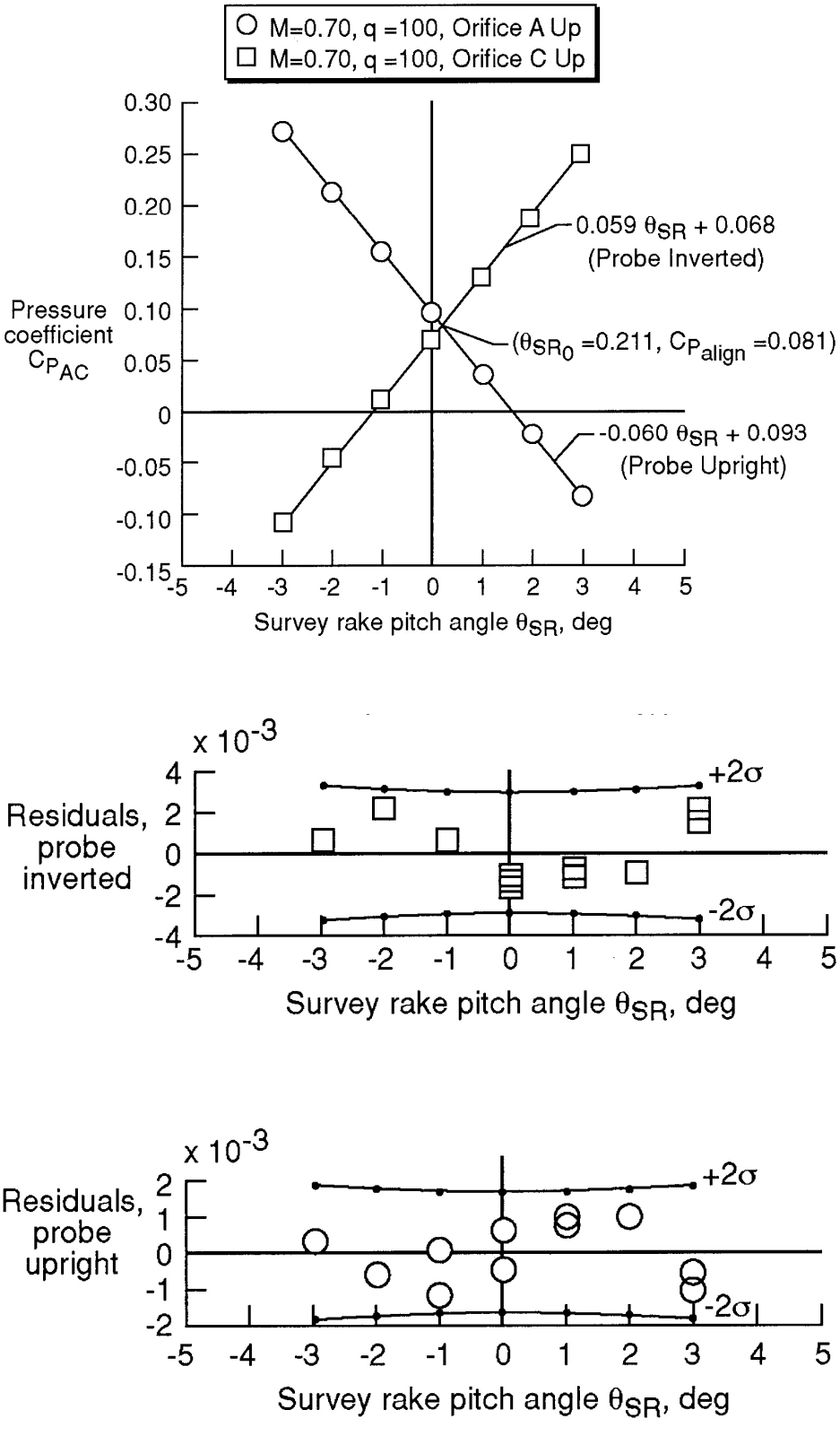

Figure 8. Representative five-hole probe calibration data.

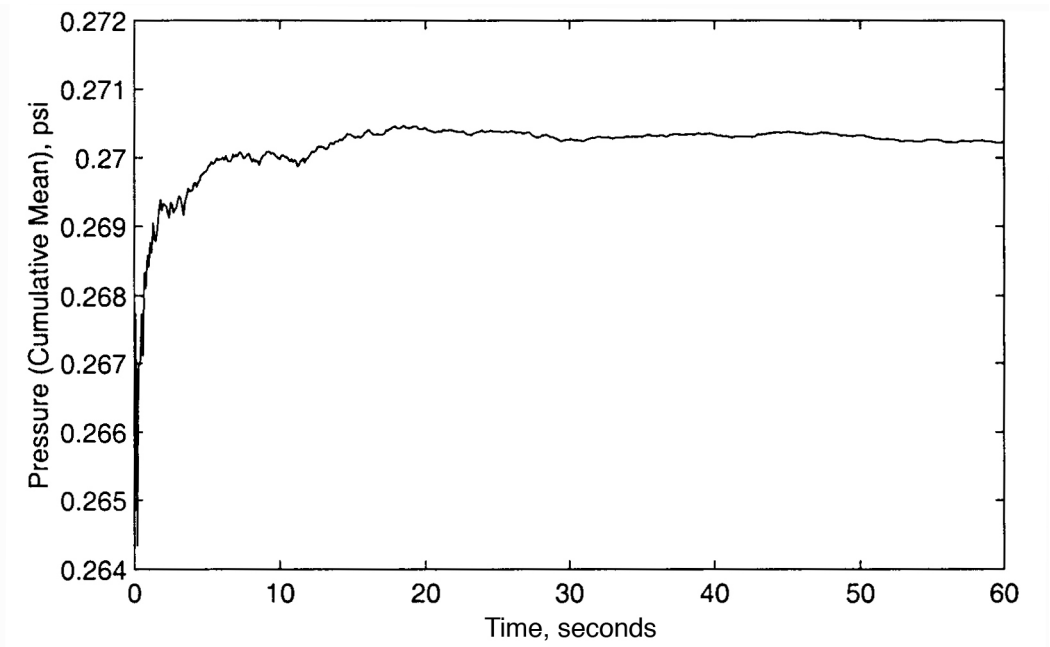

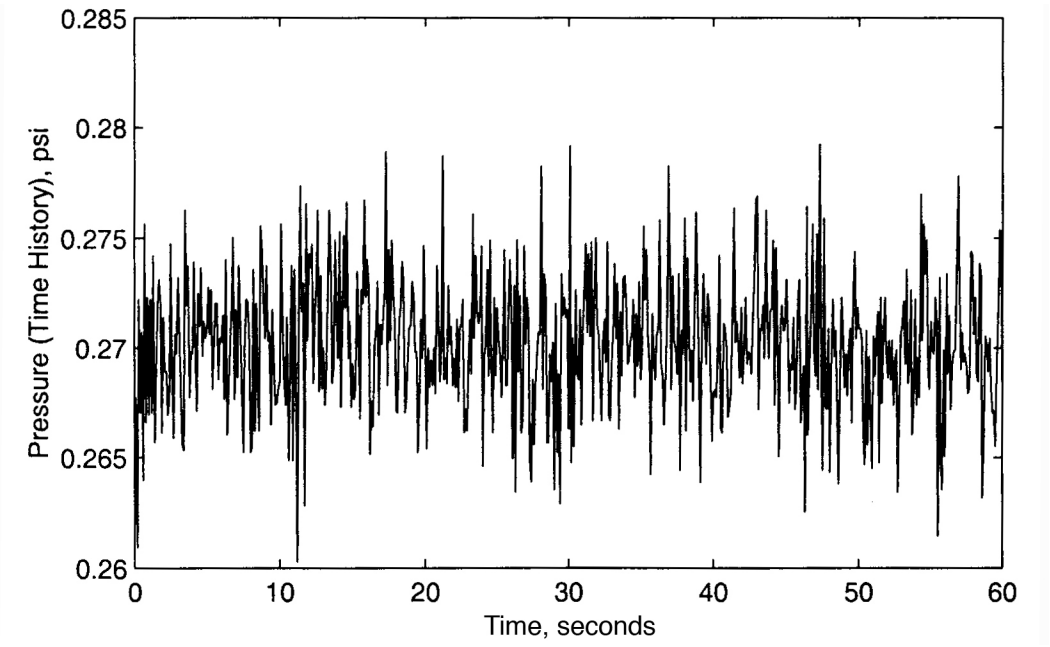

Figure 9. Representative data used for establishing data acqusition duration.

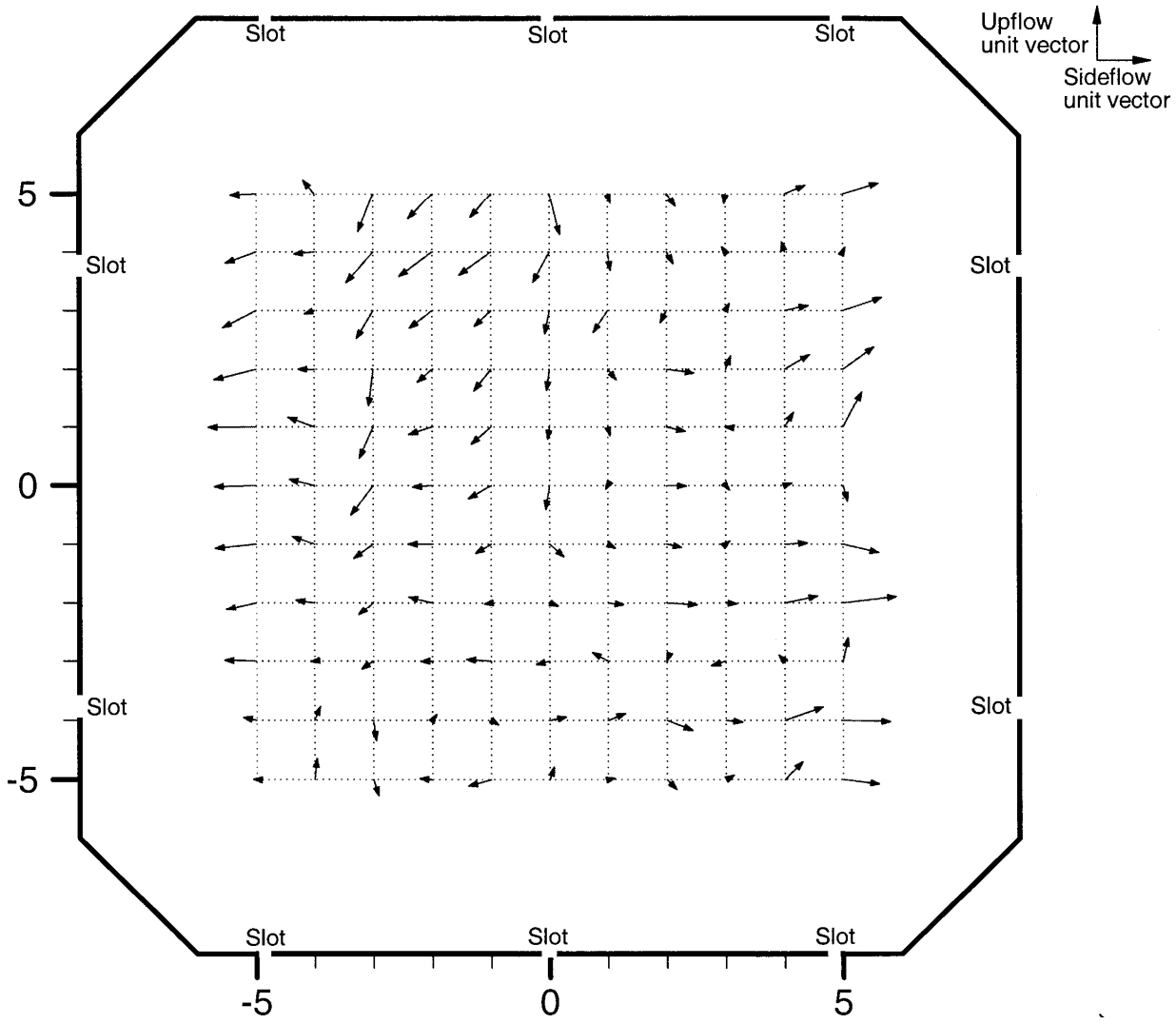

(a) M = 0.5

Figure 10. Test section flow angularity map for q = 100 psf. Results are presented looking upstream. Five-hole probe positioning locations are presented in feet, i.e., + / - 5 feet.

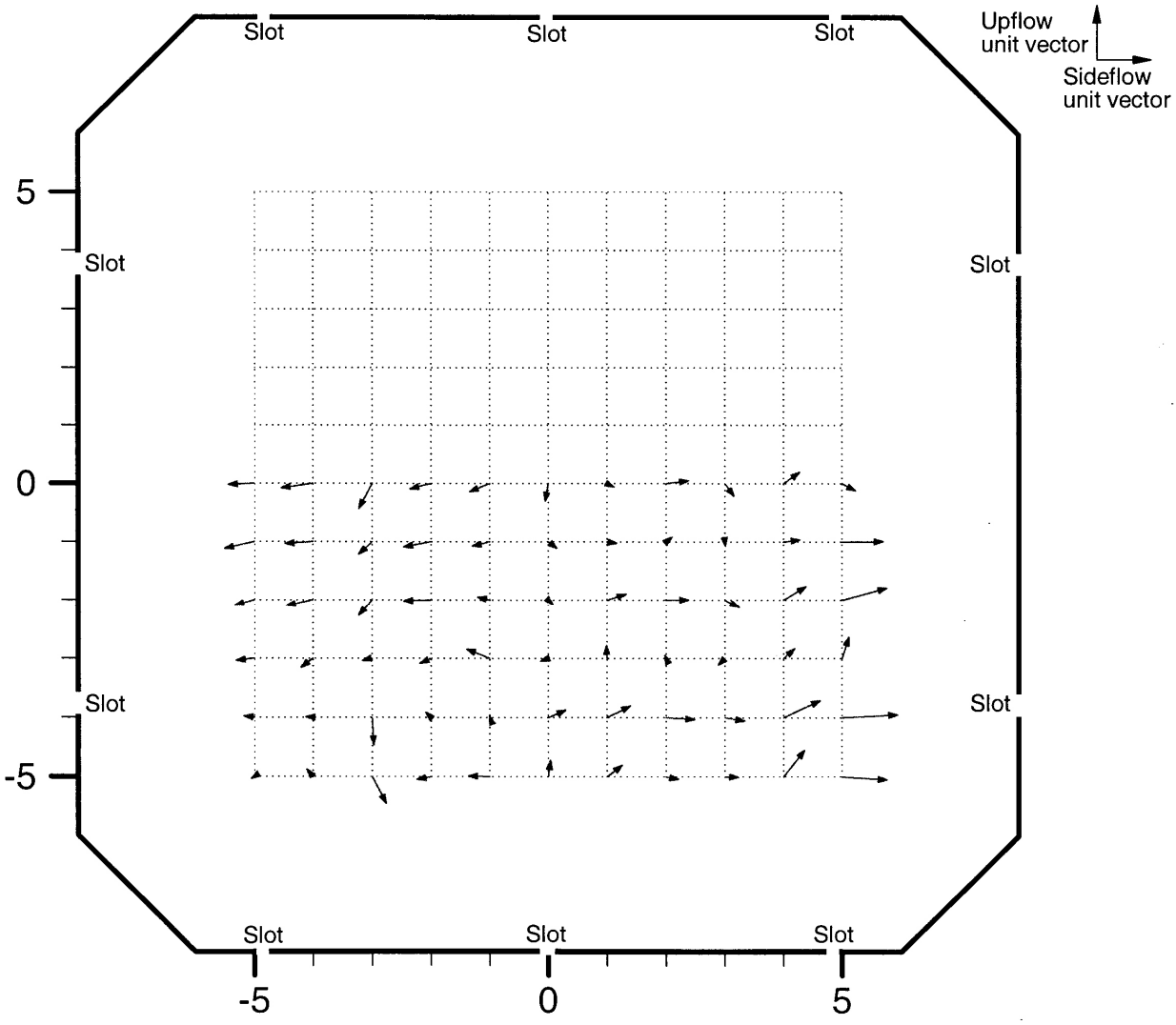

(b) M = 0.70

Figure 10. Continued.

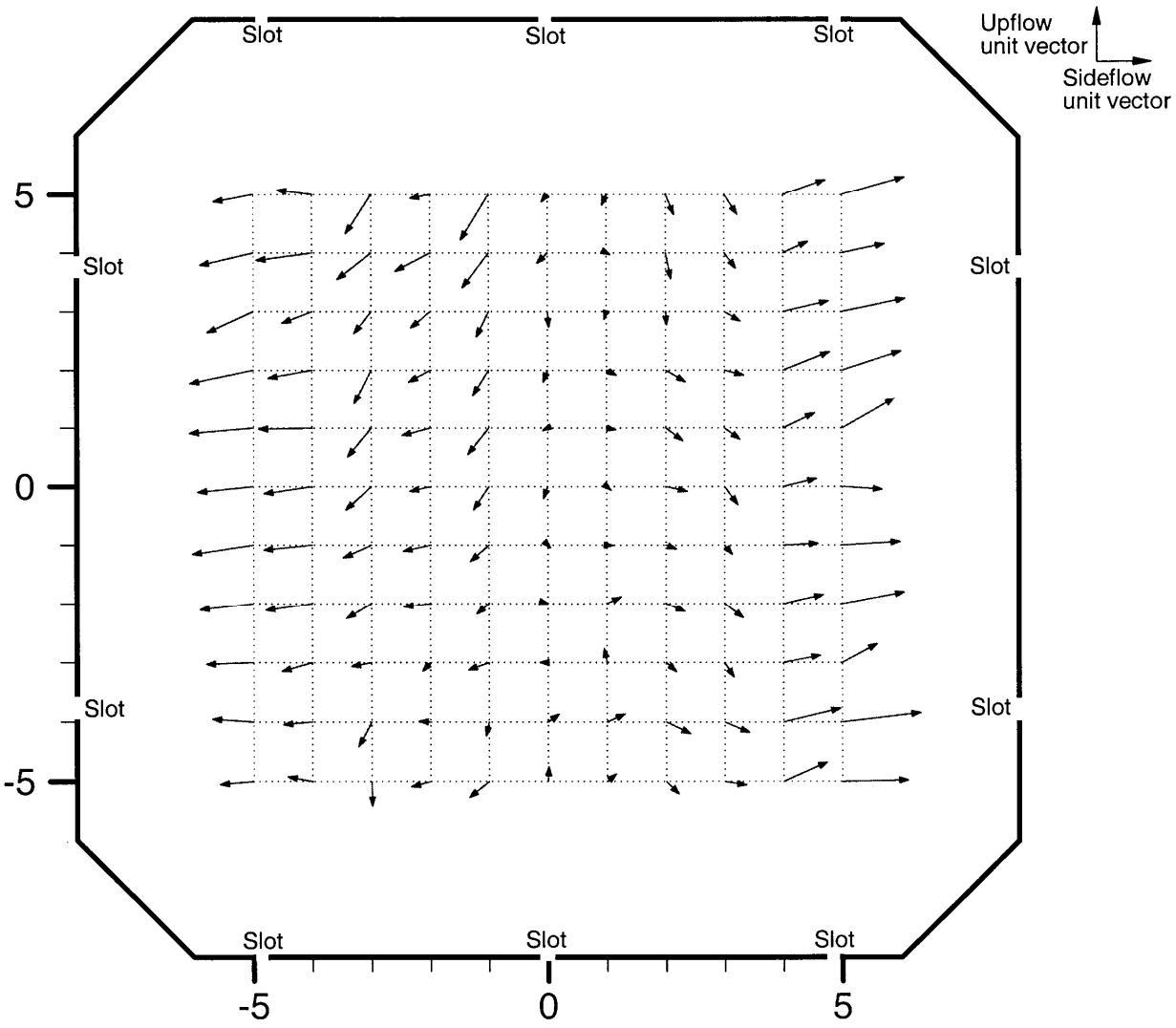

(c) M = 0.85

Figure 10. Continued.

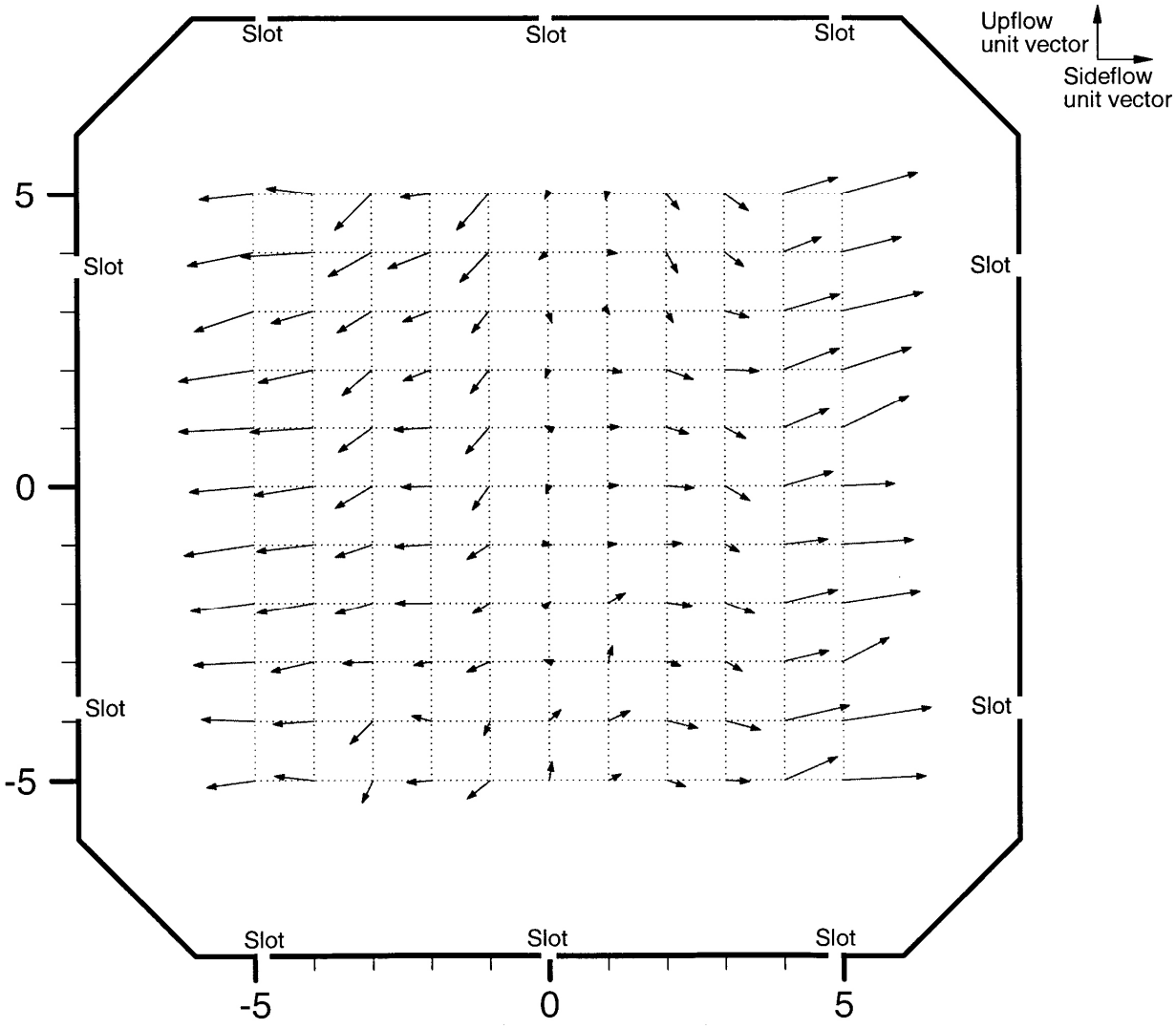

(d) M = 0.90

Figure 10. Continued.

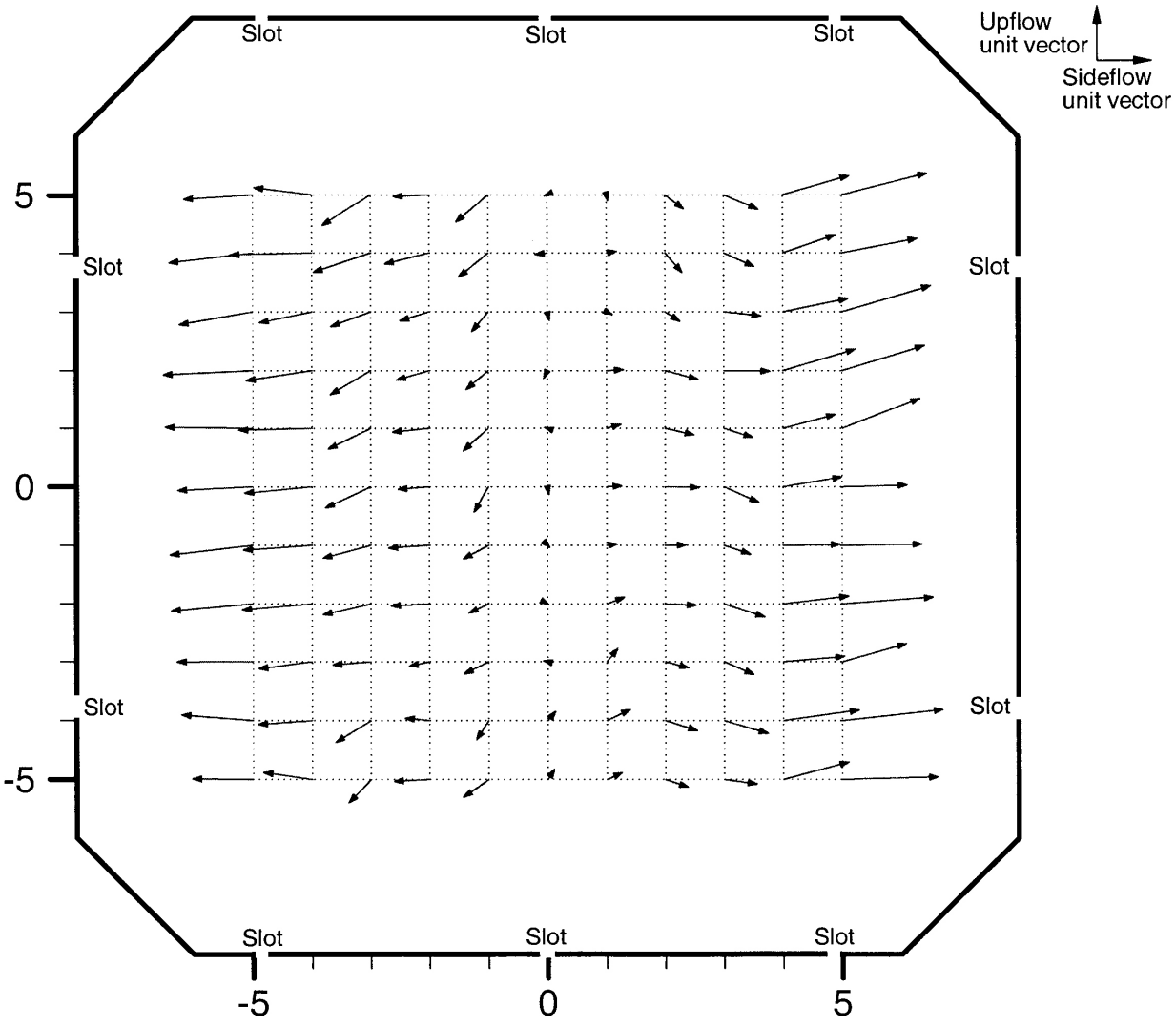

(e) M = 0.95

Figure 10. Continued.

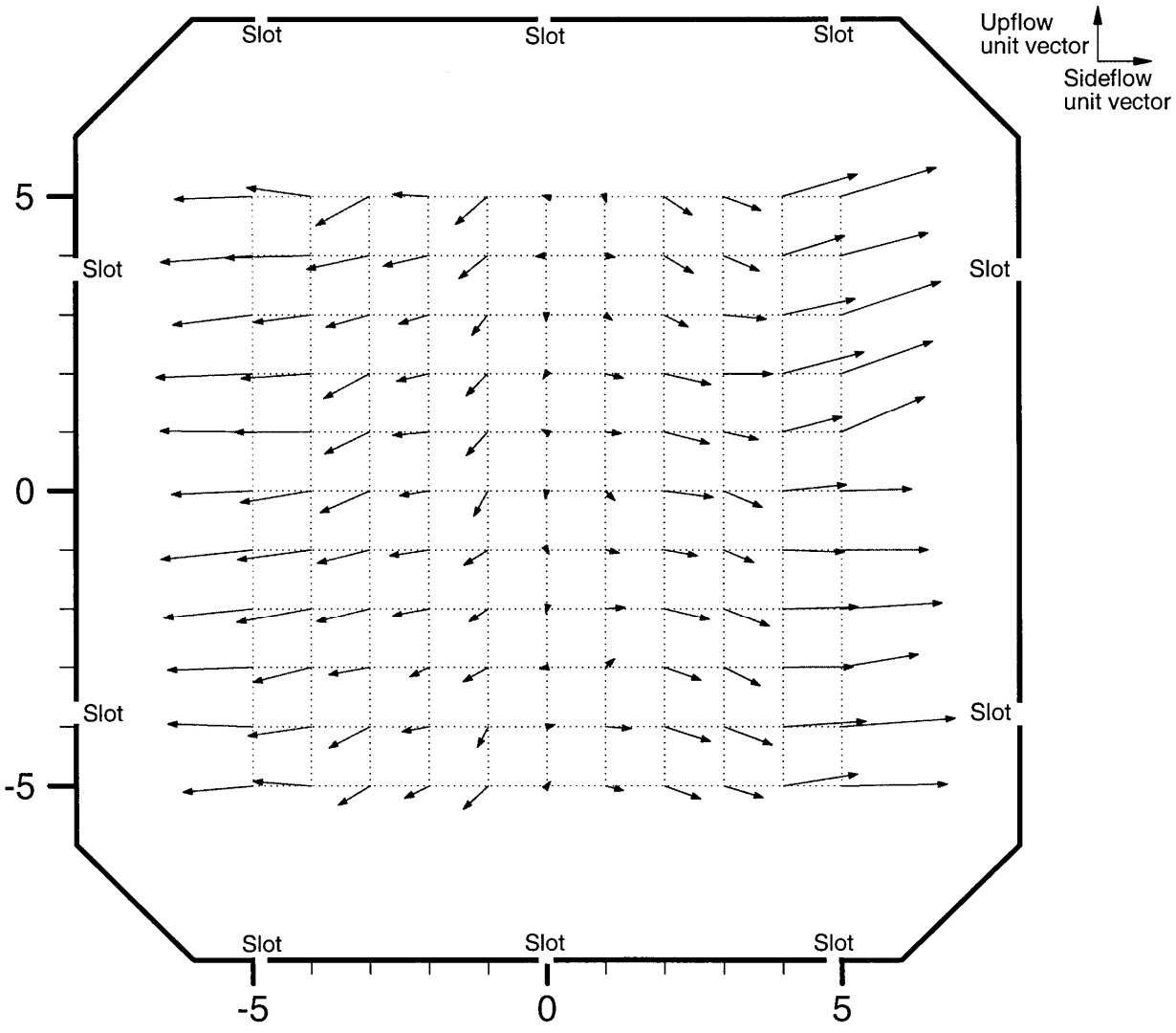

(f) M = 1.00

Figure 10. Continued.

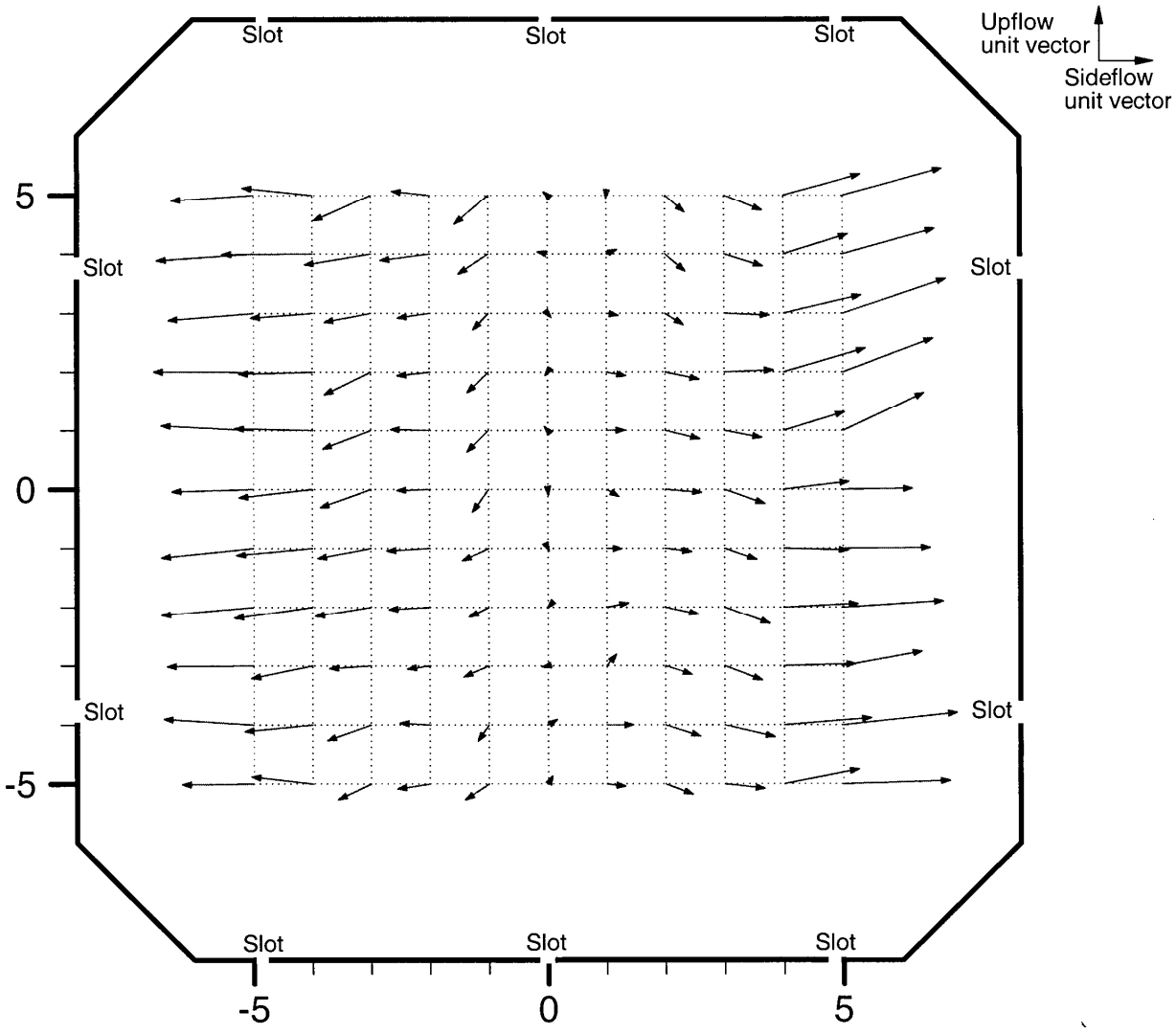

(g) M = 1.05

Figure 10. Continued.

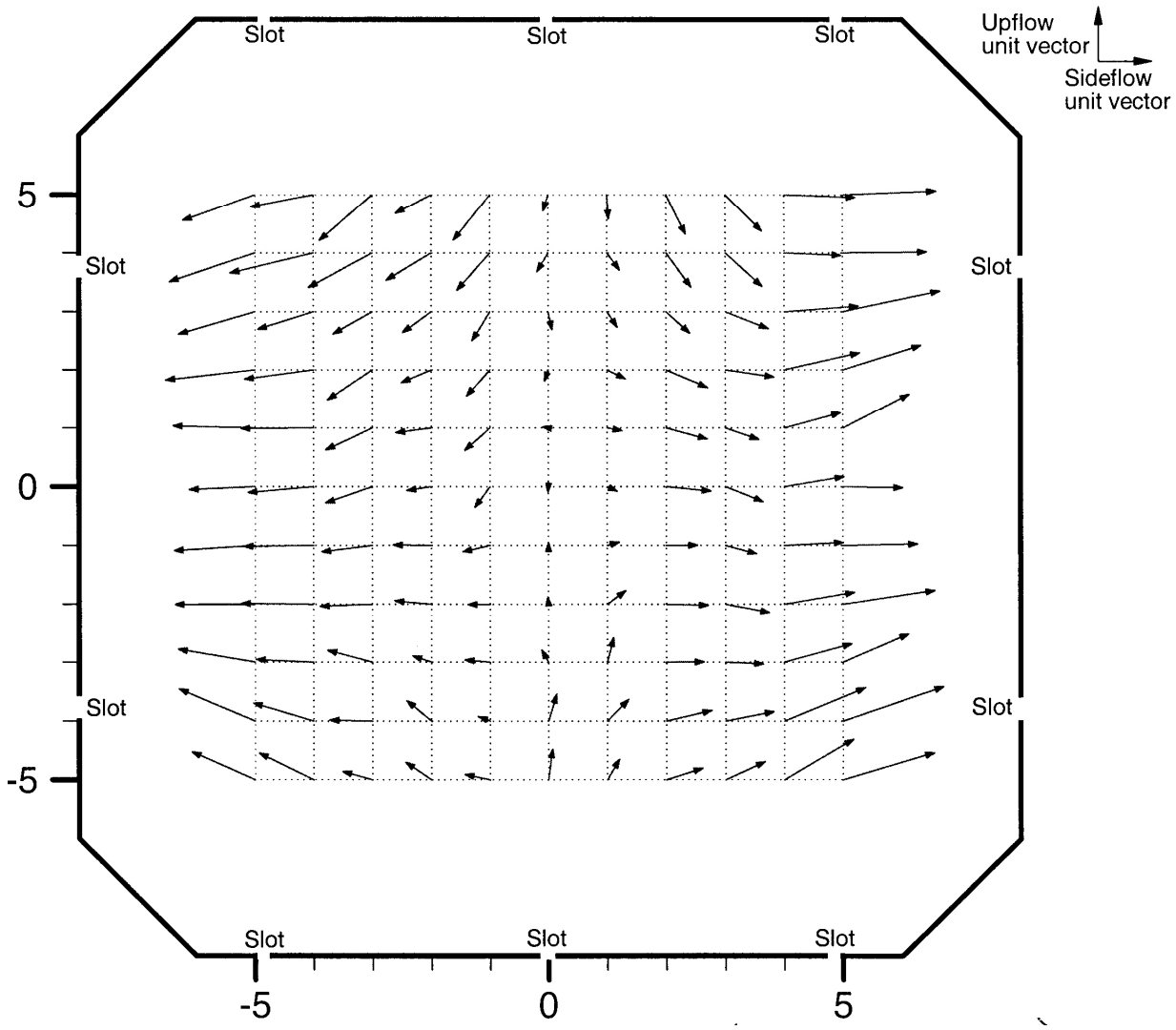

(h) M = 1.10

Figure 10. Continued.

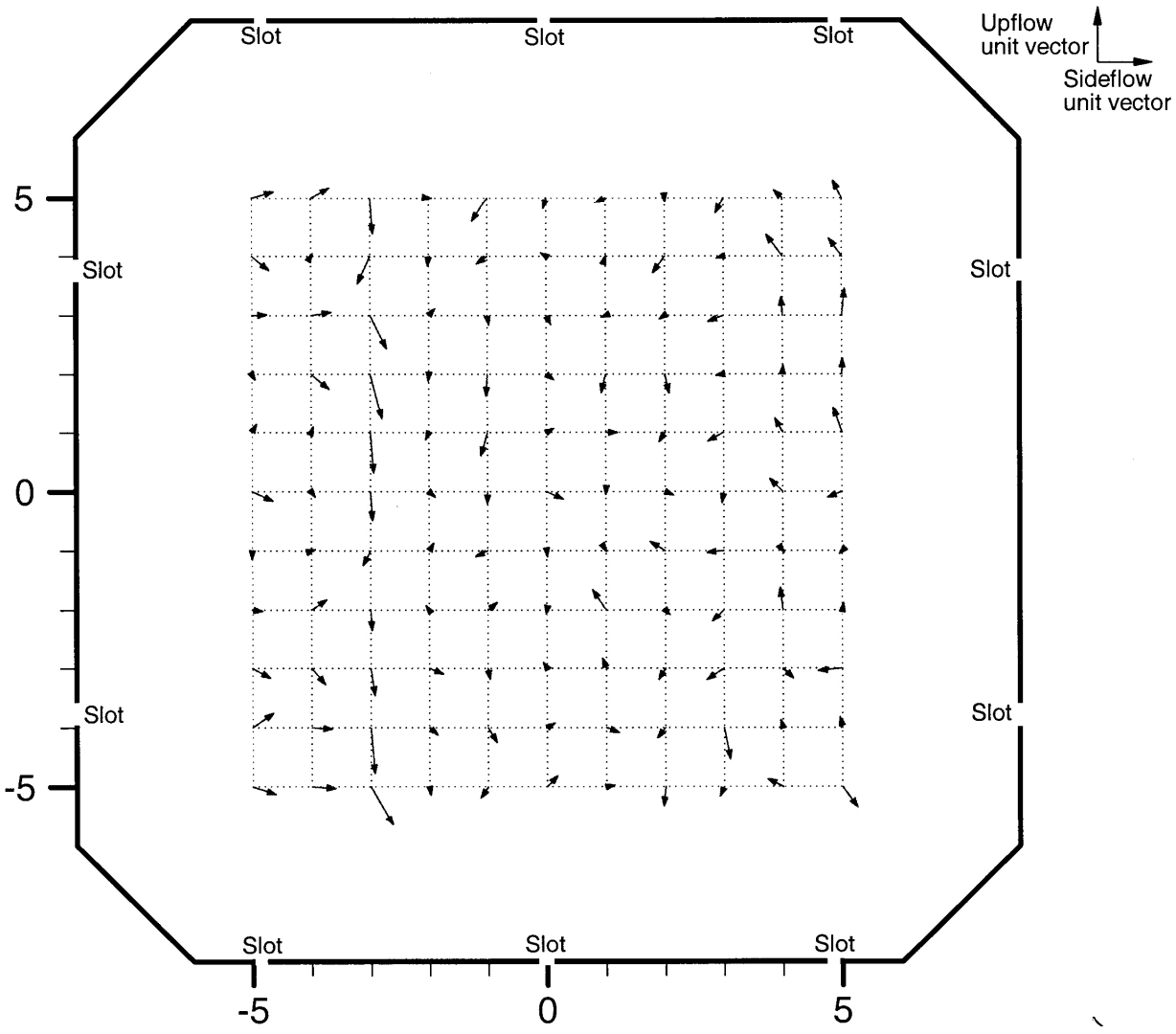

(i) M = 1.19

Figure 10. Concluded.

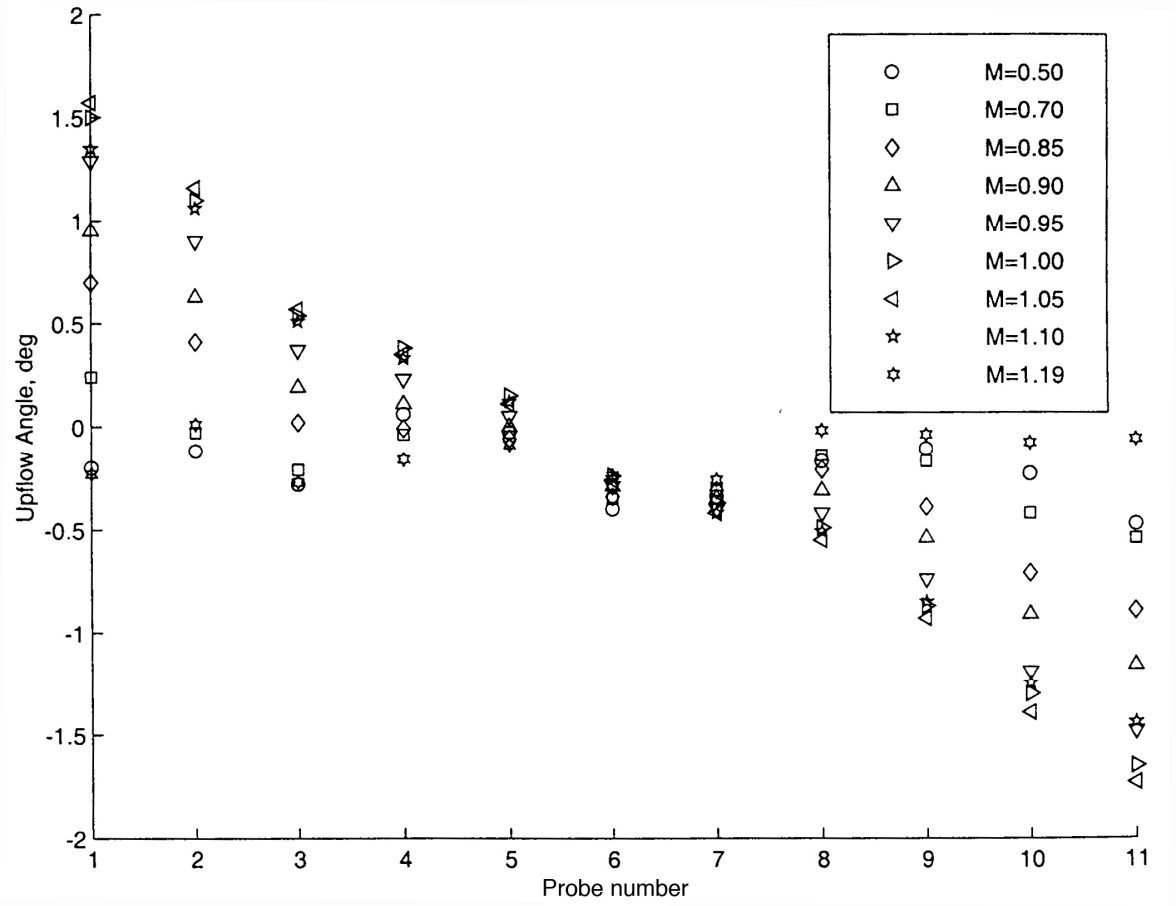

(a) q = 100 psf

Figure 11. Upflow as measured by five-hole probe orifices A and C with survey rake in probe calibration (vertical) orientation. Probe number refers to five-hole probe location on survey rake as viewed from above (see Figure 4 (b)).

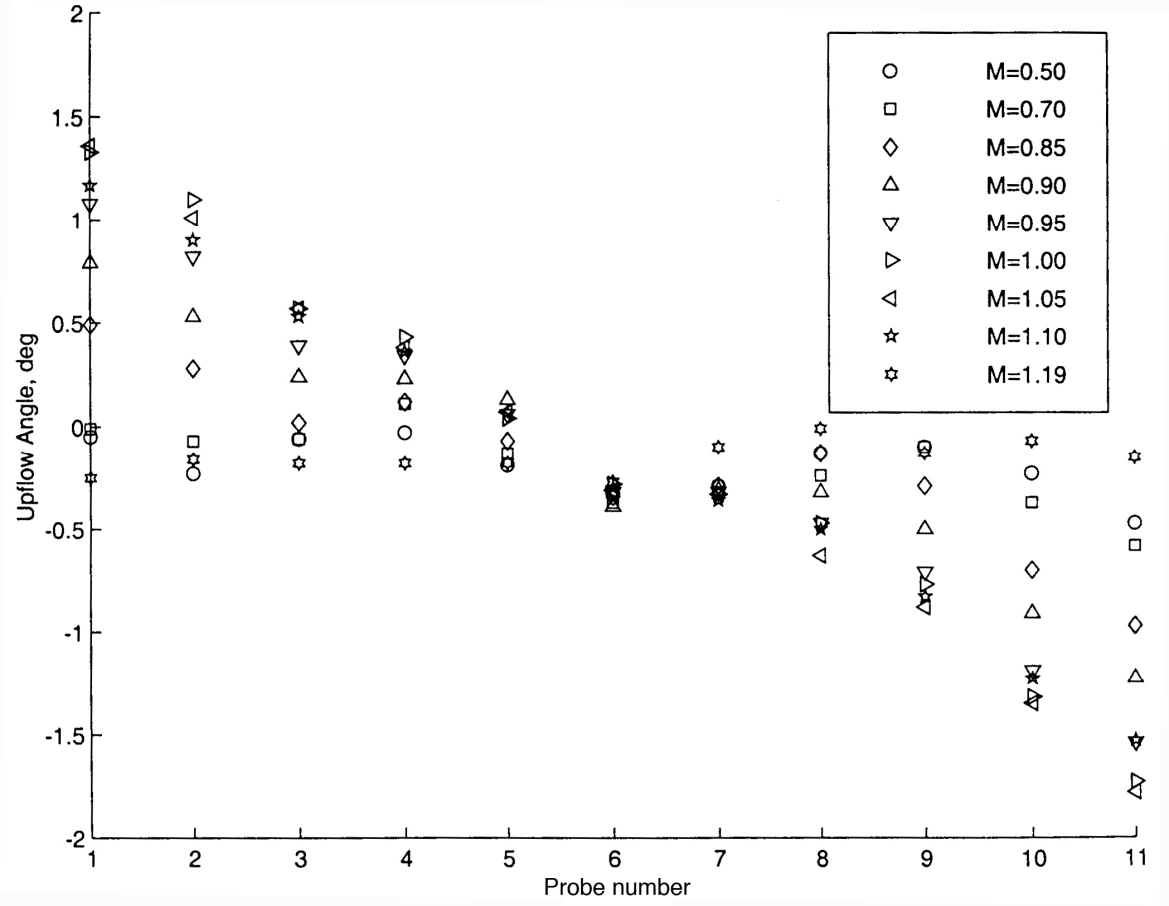

(b) q = 225 psf

Figure 11. Concluded.

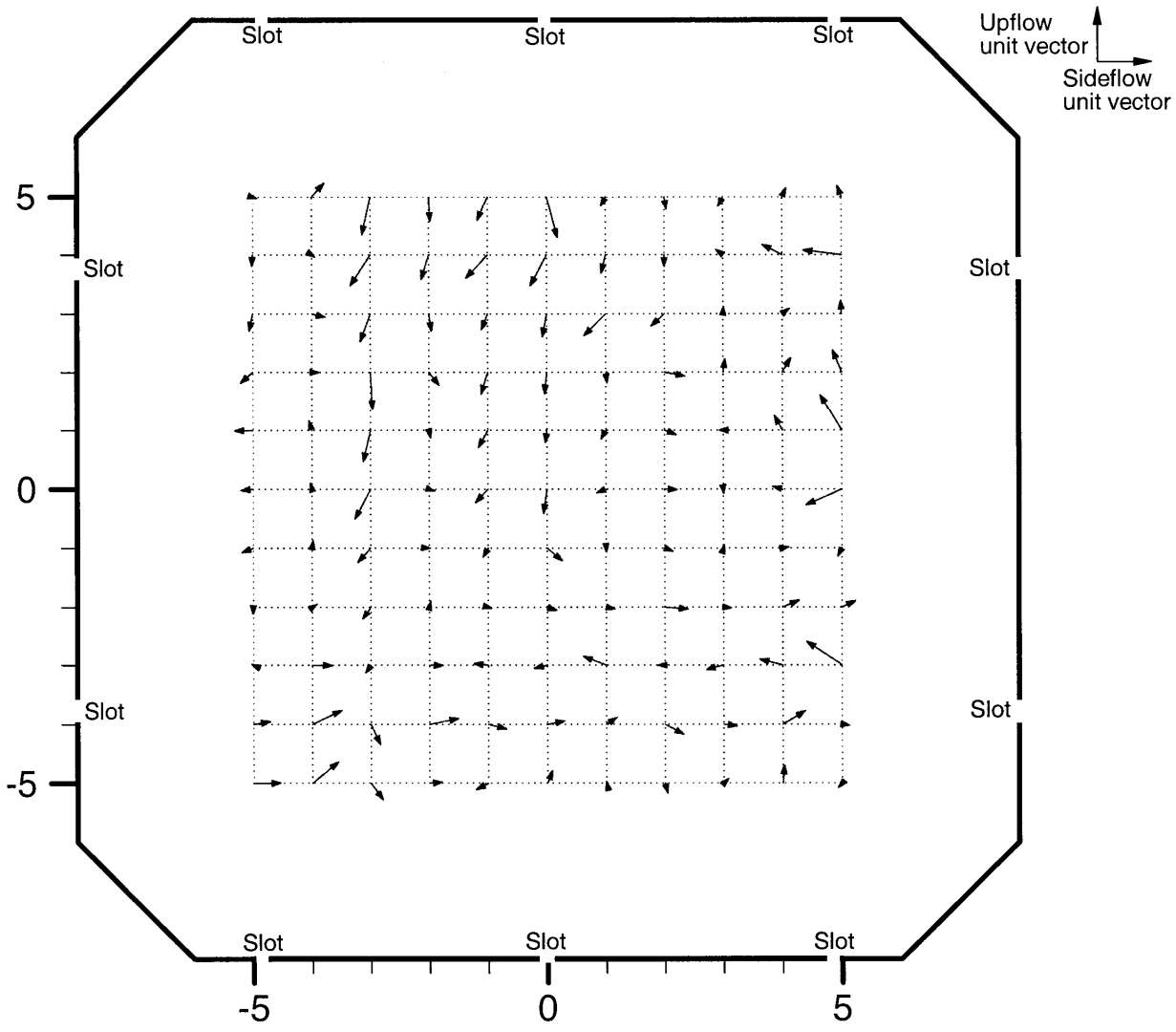

(a) M = 0.50

Figure 12. Flow angularity maps for q = 100 psf with sideflow corrections. Results are presented looking upstream. Five-hole probe positioning locations are presented in feet, i.e., + / - 5 feet.

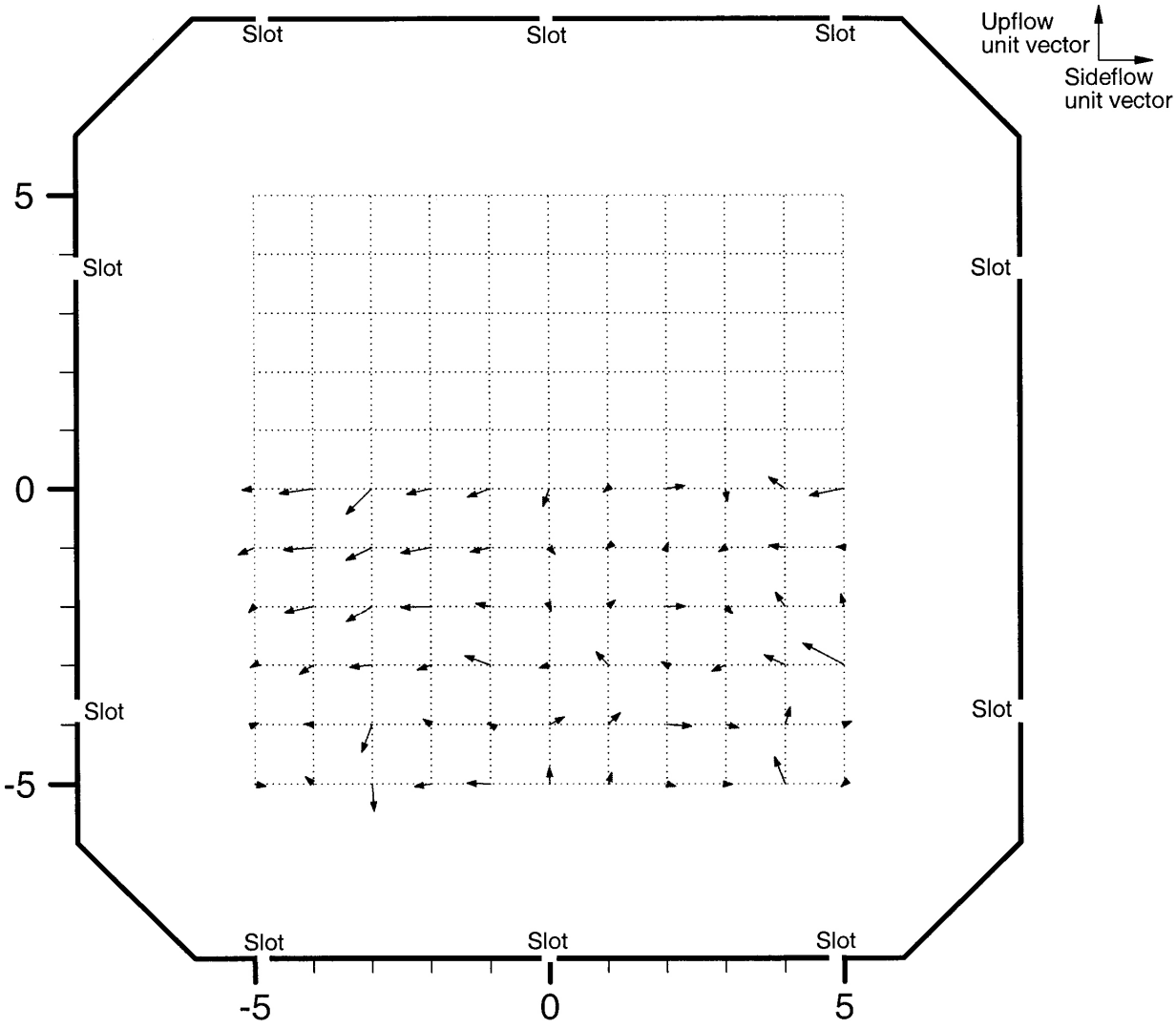

(b) M = 0.70

Figure 12. Continued.

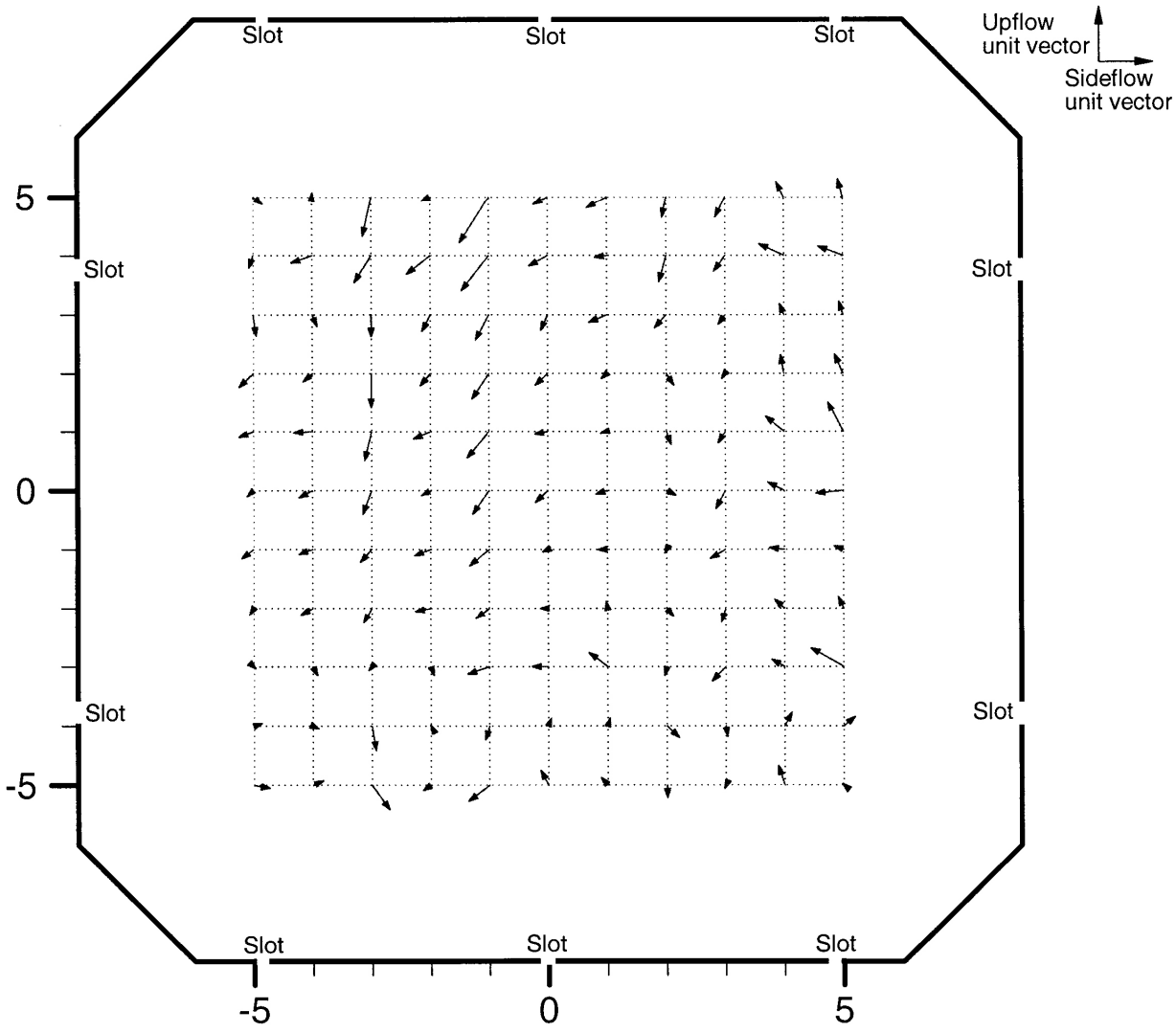

(c) M = 0.85

Figure 12. Continued.

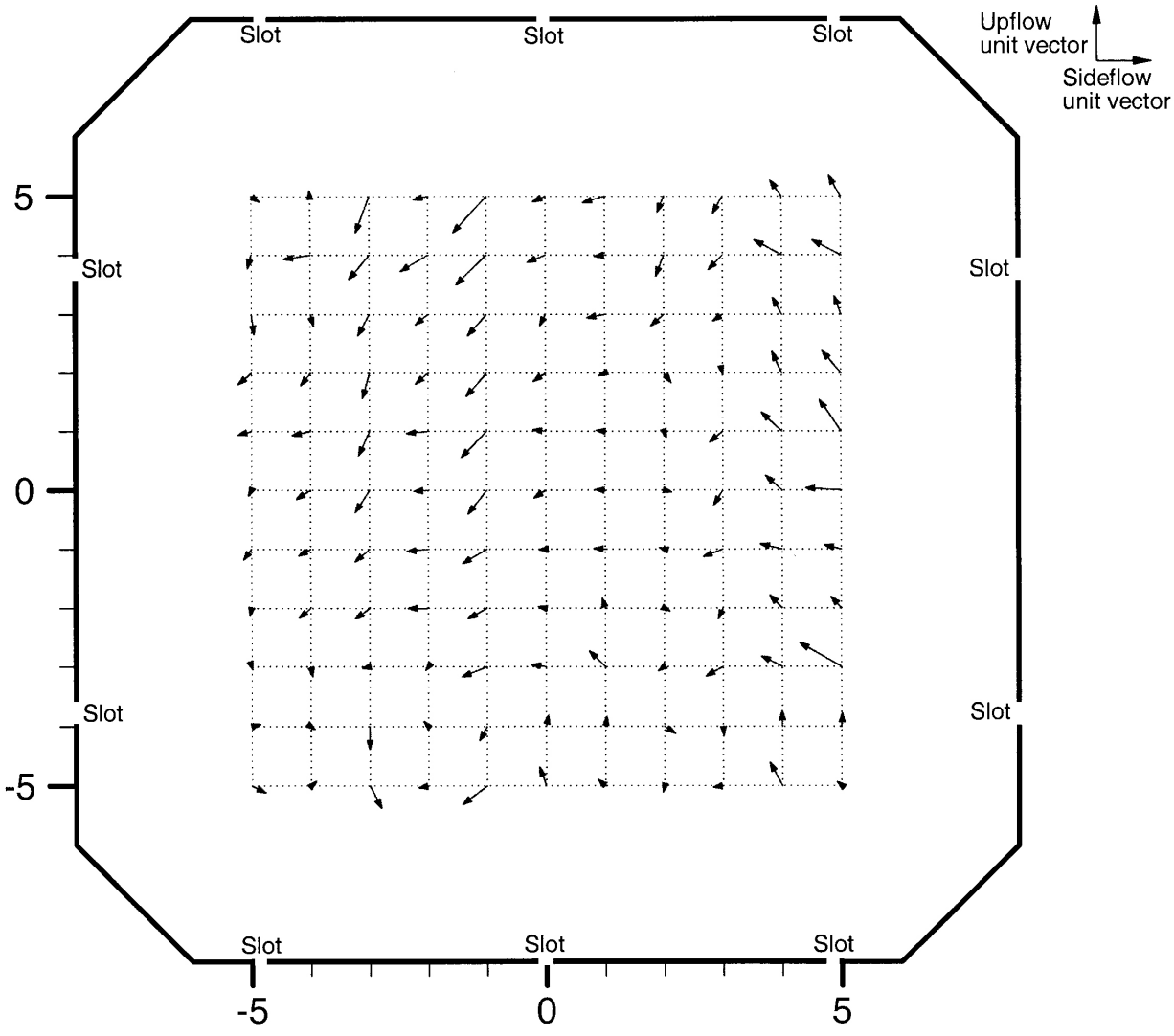

(d) M = 0.90

Figure 12. Continued.

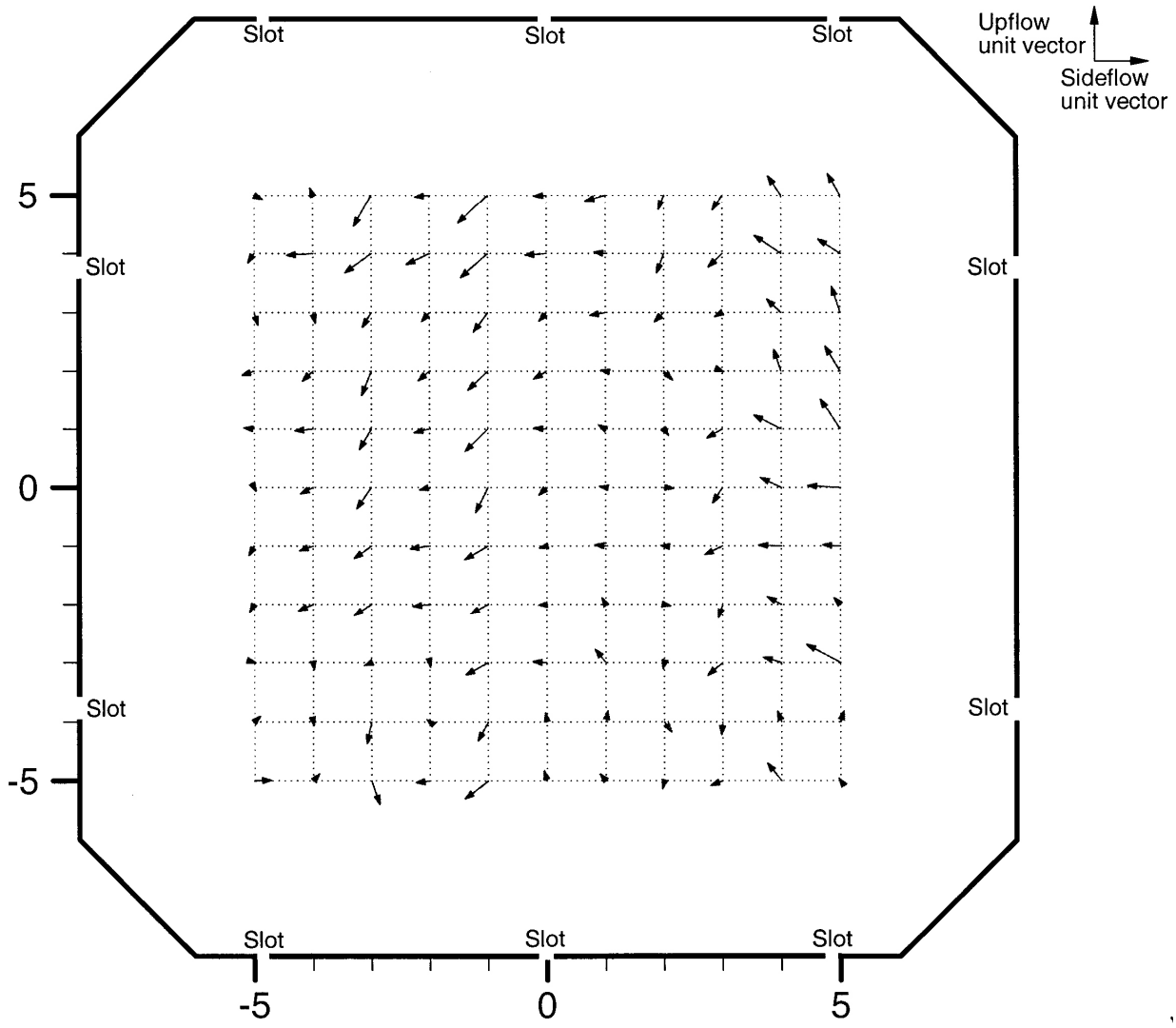

(e) M = 0.95

Figure 12. Continued.

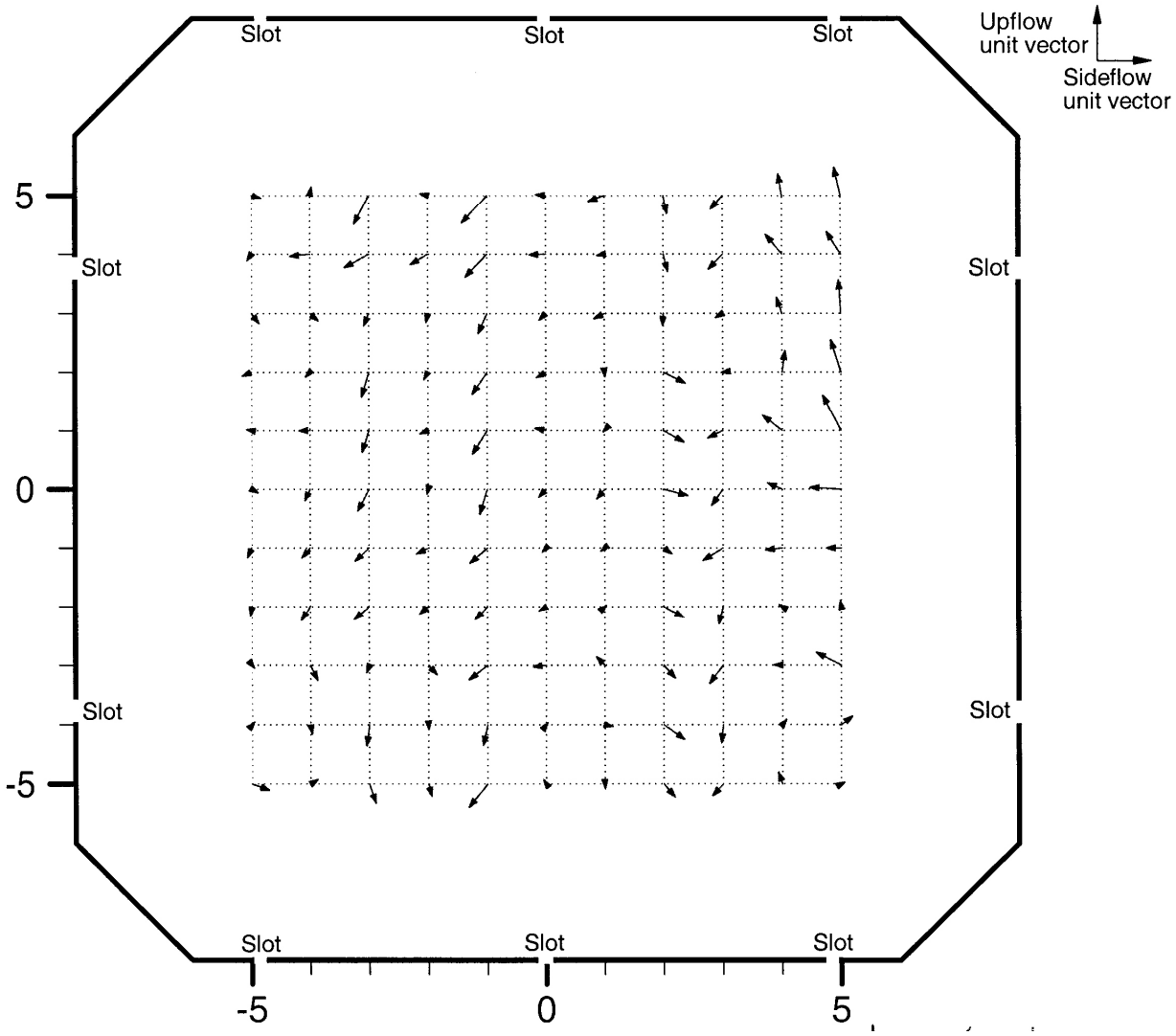

(f) M = 1.00

Figure 12. Continued.

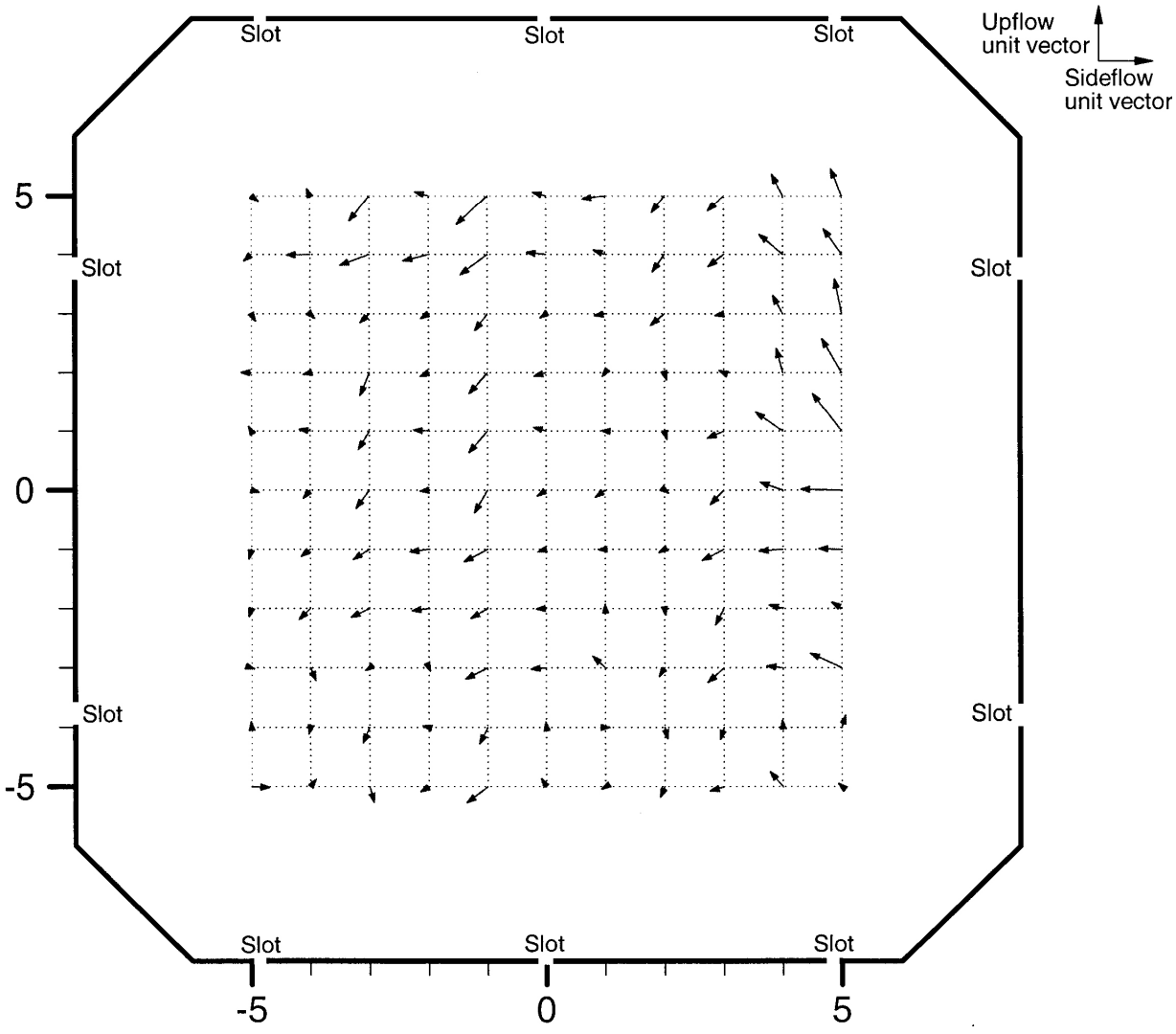

(g) M = 1.05

Figure 12. Continued.

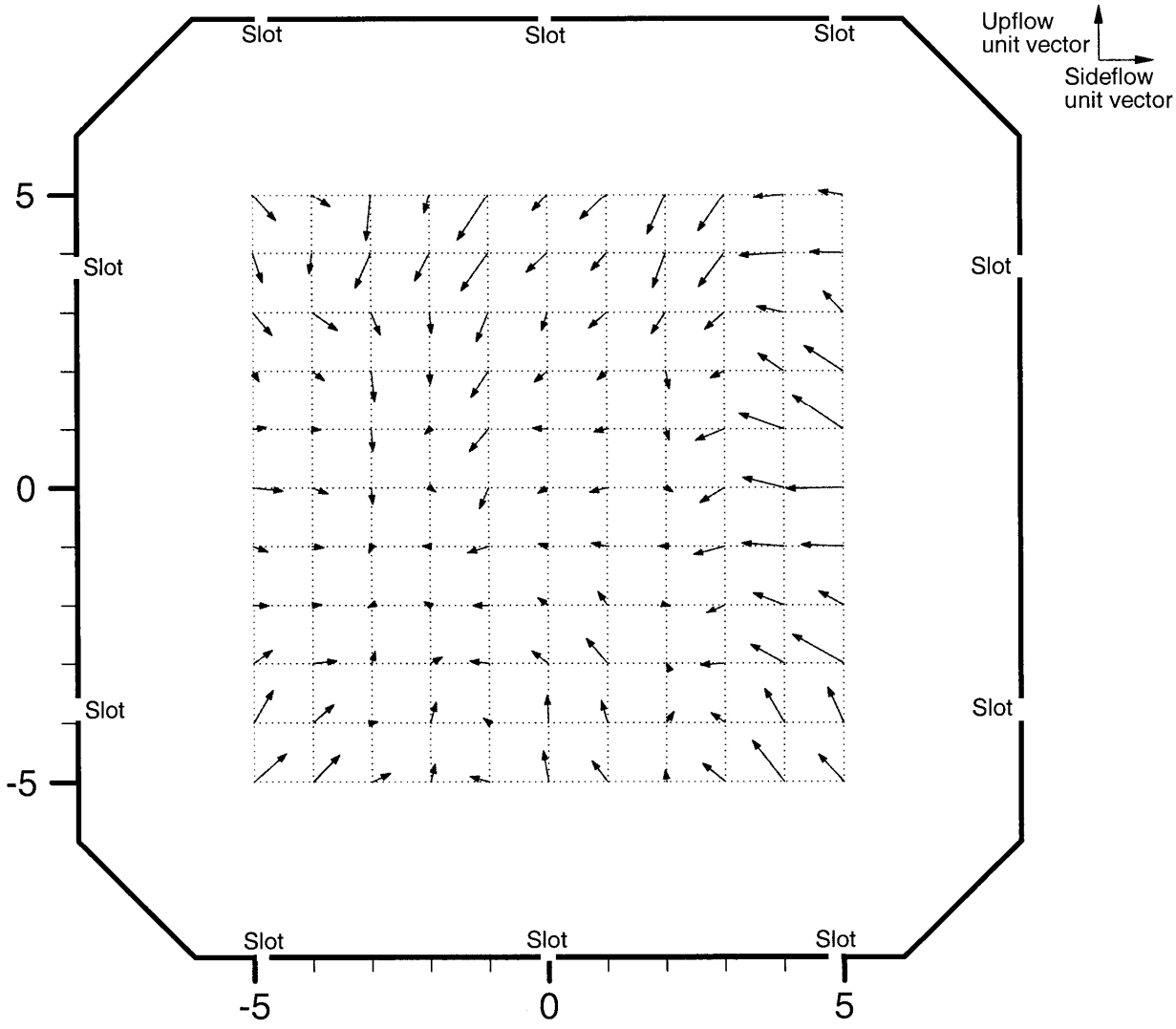

(h) M = 1.10

Figure 12. Continued.

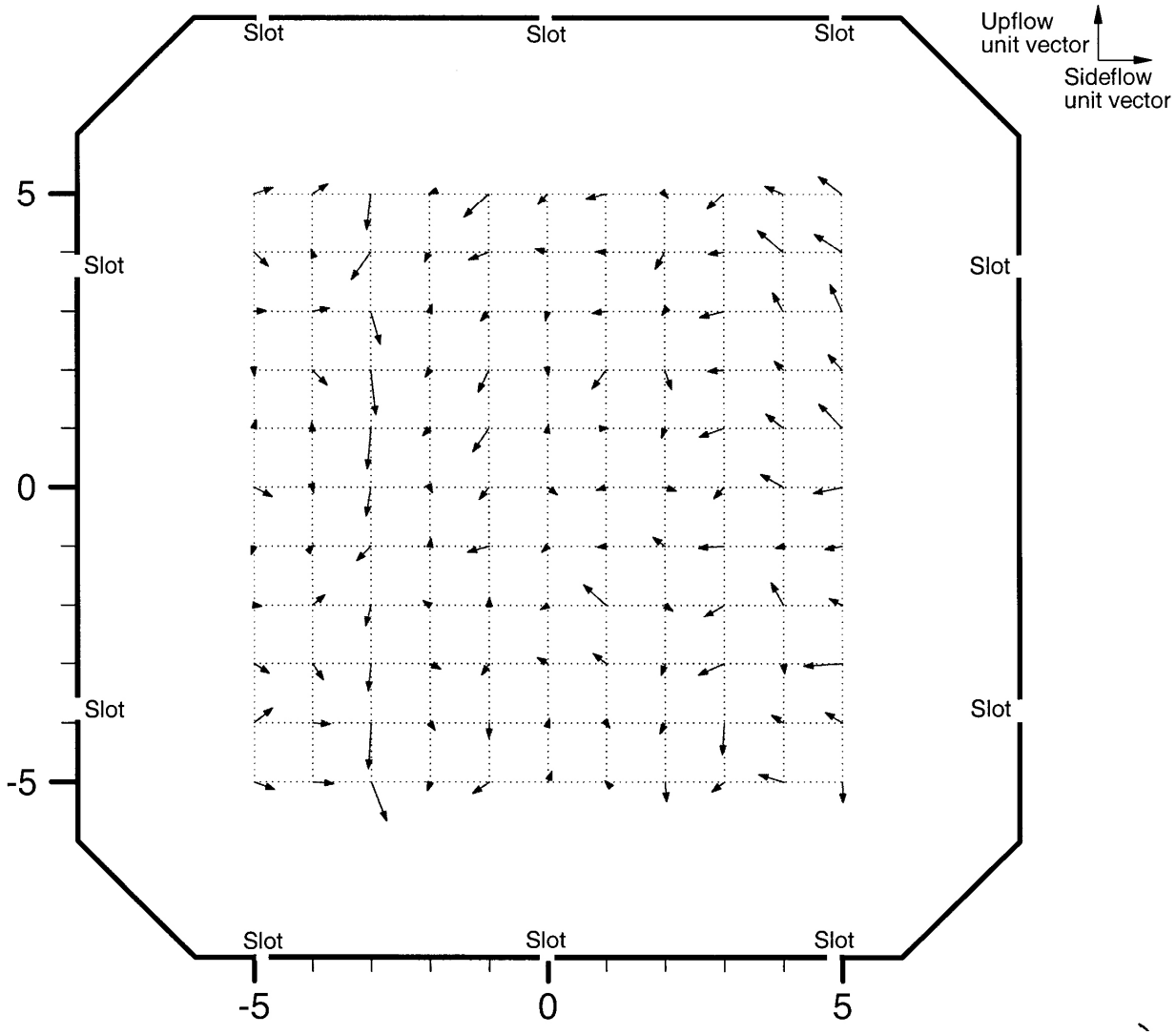

(i) M = 1.19

Figure 12. Concluded.

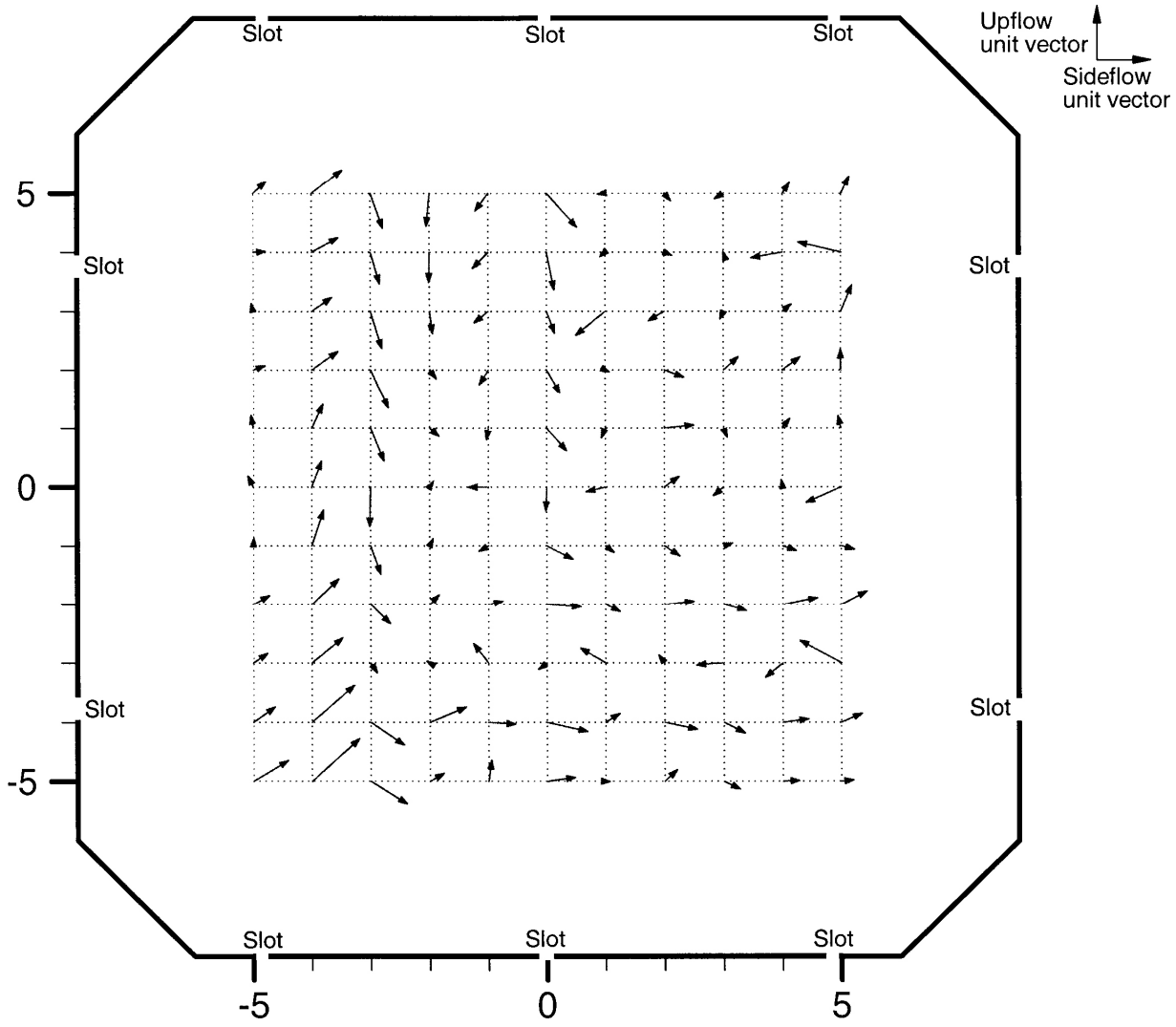

(a) M = 0.50

Figure 13. Flow angularity maps for q = 225 psf with sideflow corrections. Results are presented looking upstream. Five-hole probe positioning locations are presented in feet, i.e., + / - 5 feet.

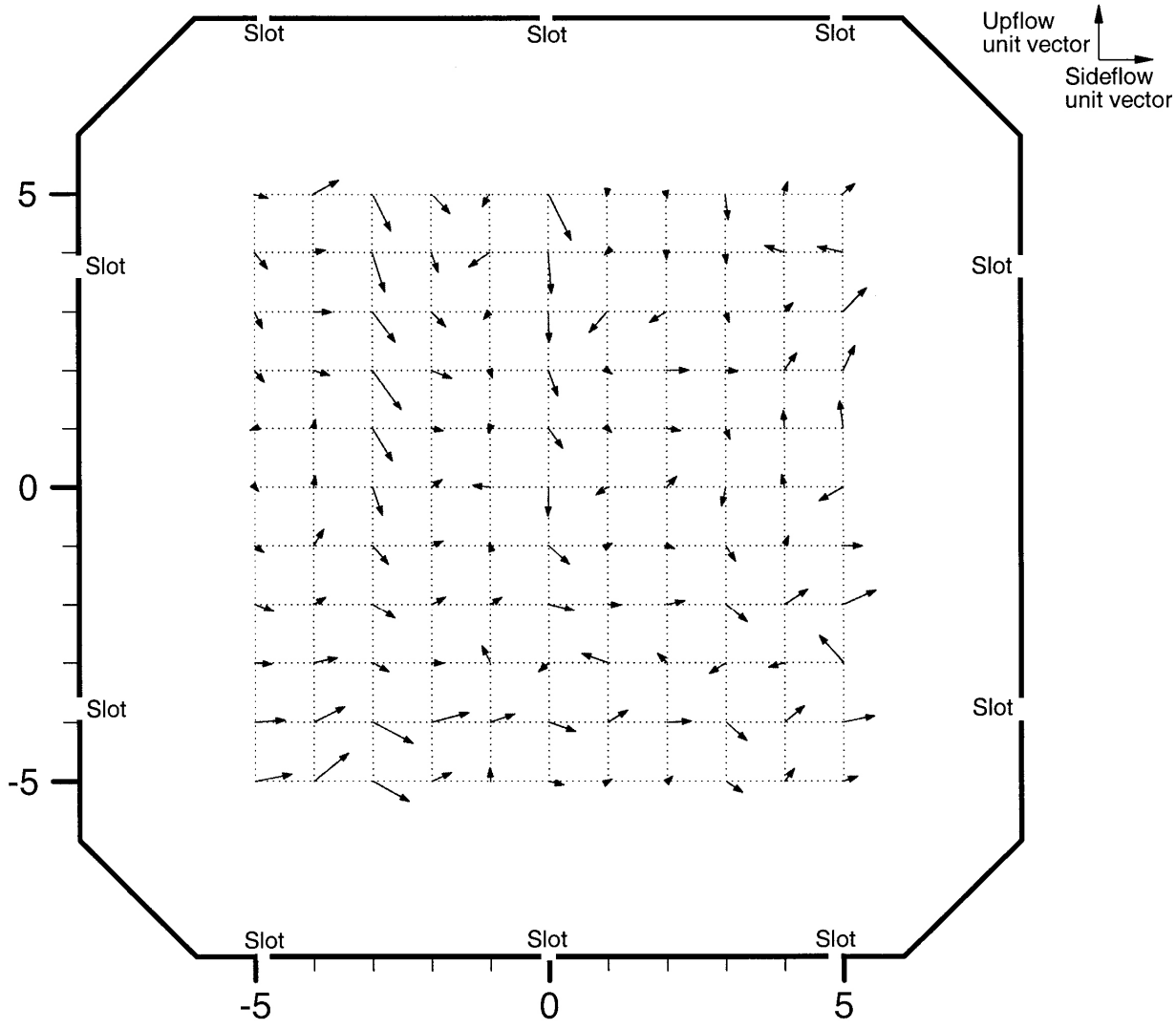

(b) M = 0.70

Figure 13. Continued.

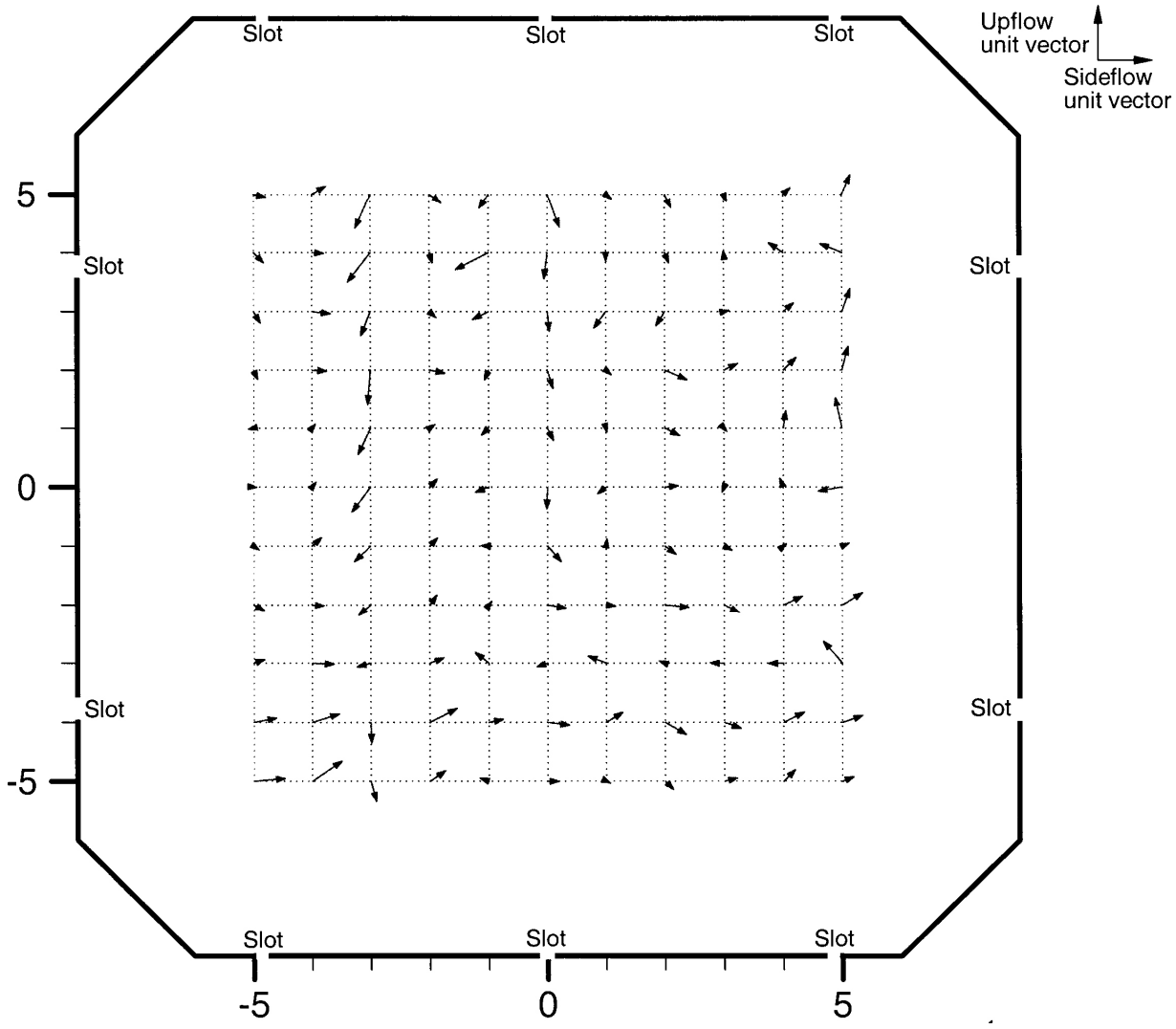

(c) M = 0.85

Figure 13. Continued.

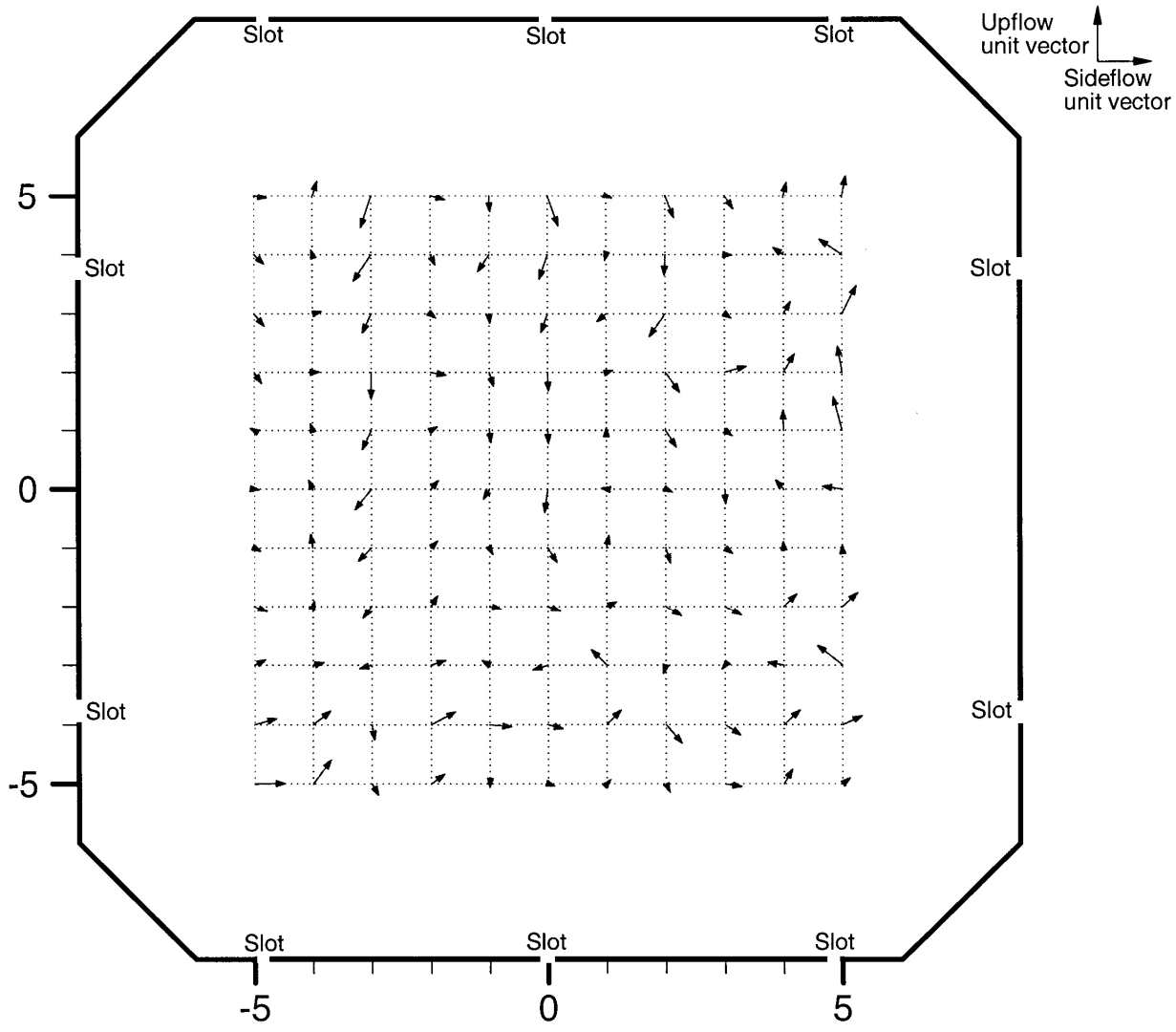

(d) M = 0.90

Figure 13. Continued.

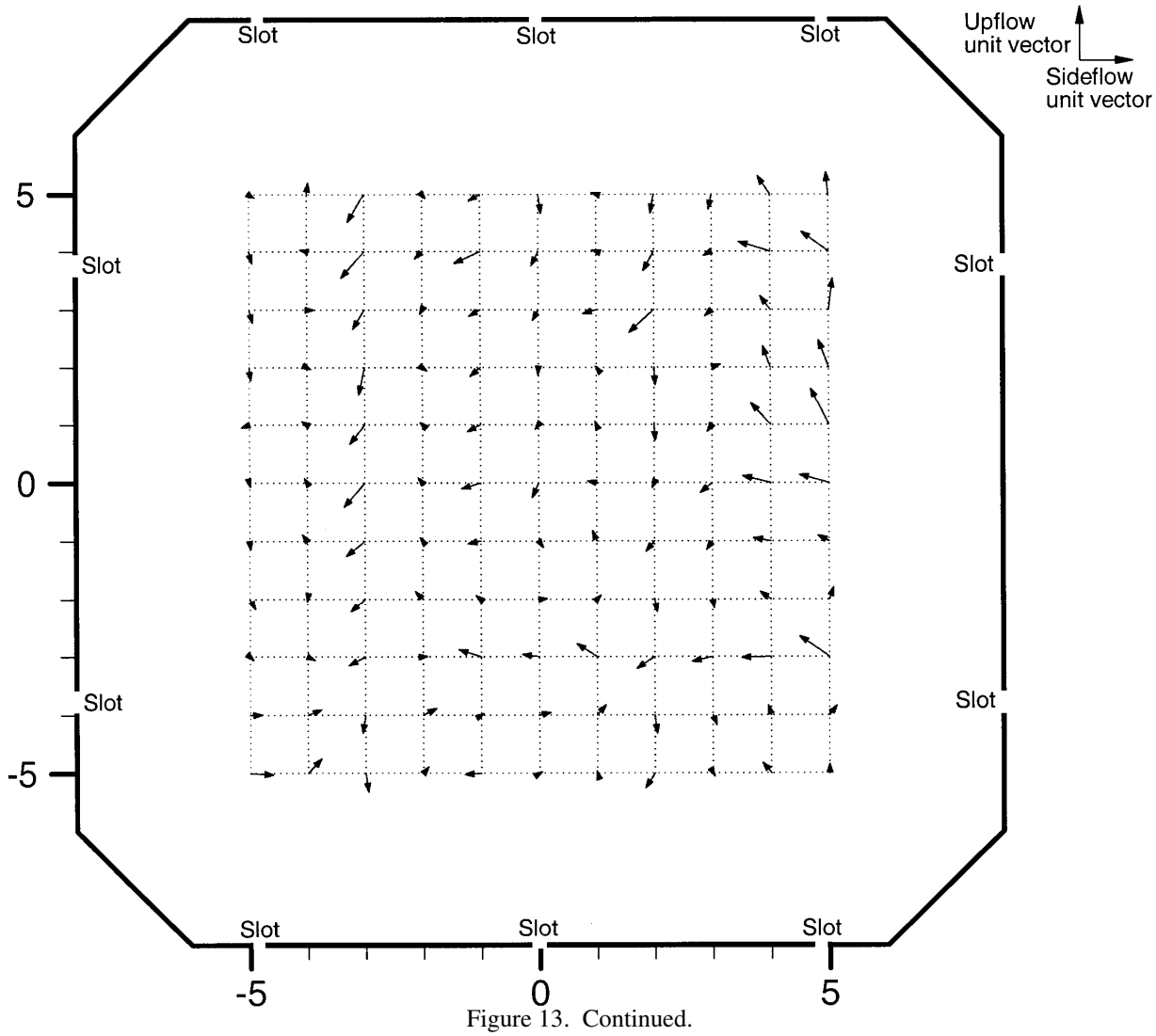

Figure 13. Continued.

(e) M = 0.95

Figure 13. Continued.

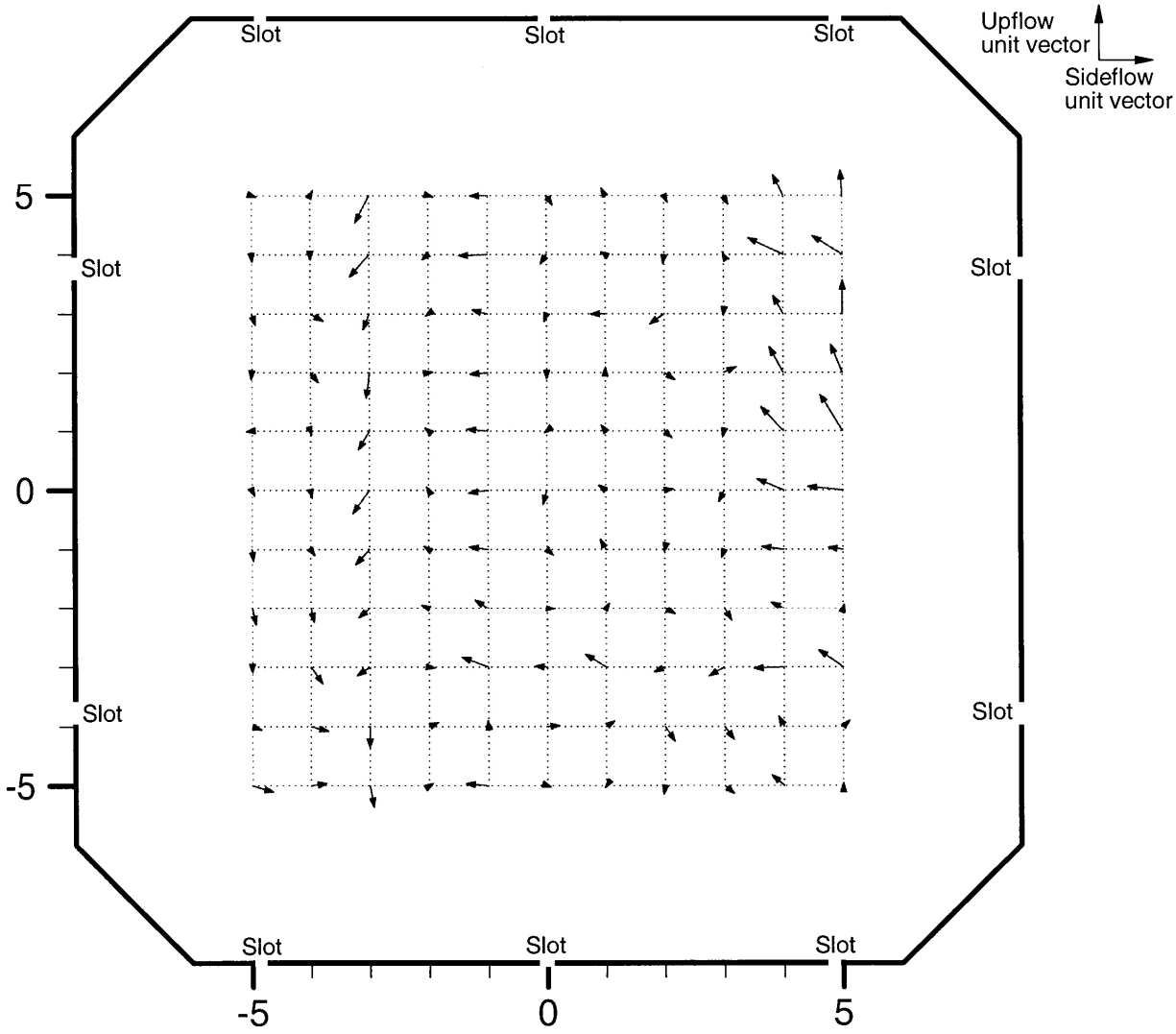

(f) M = 1.00

Figure 13. Continued.

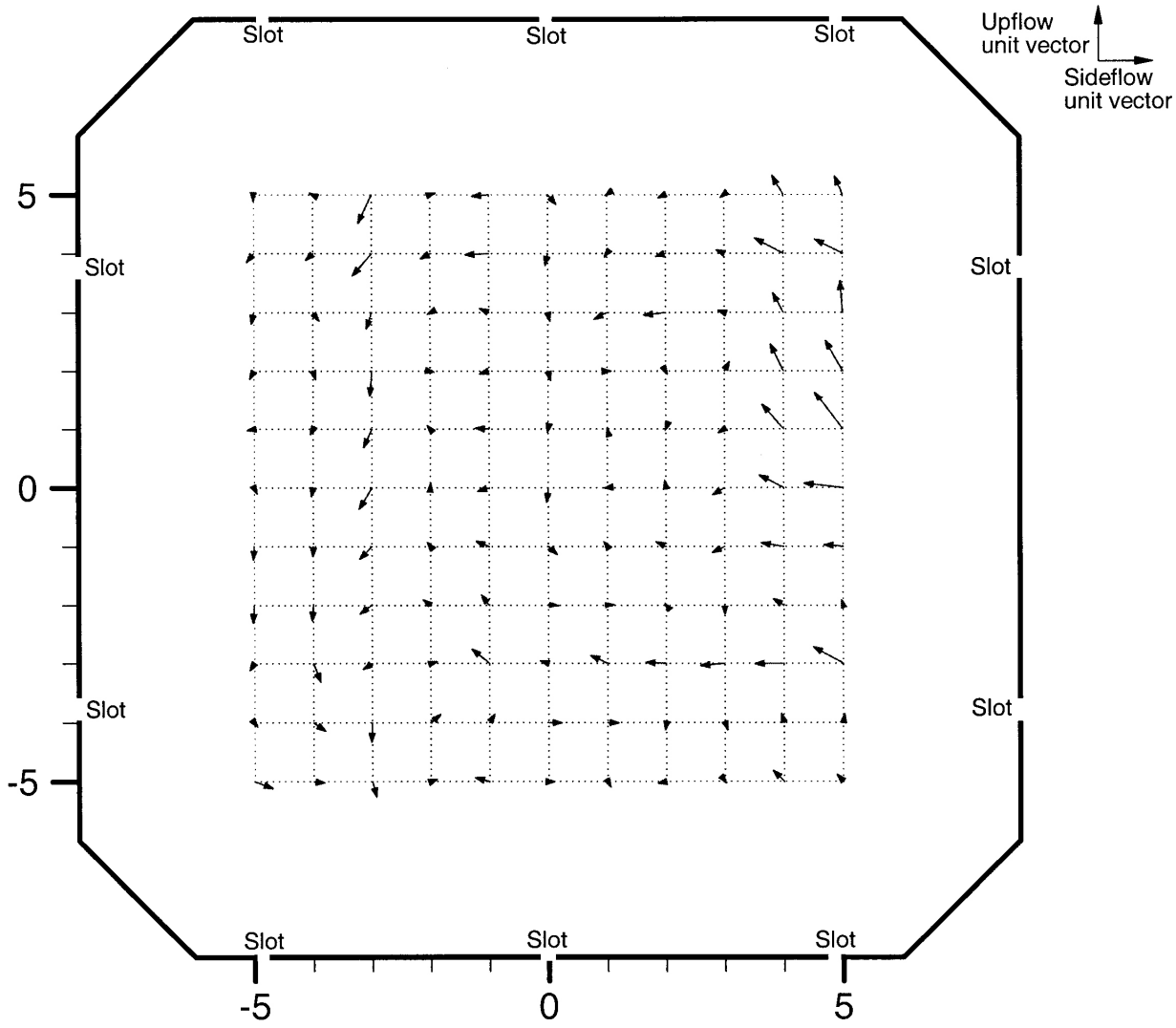

(g) M = 1.05

Figure 13. Continued.

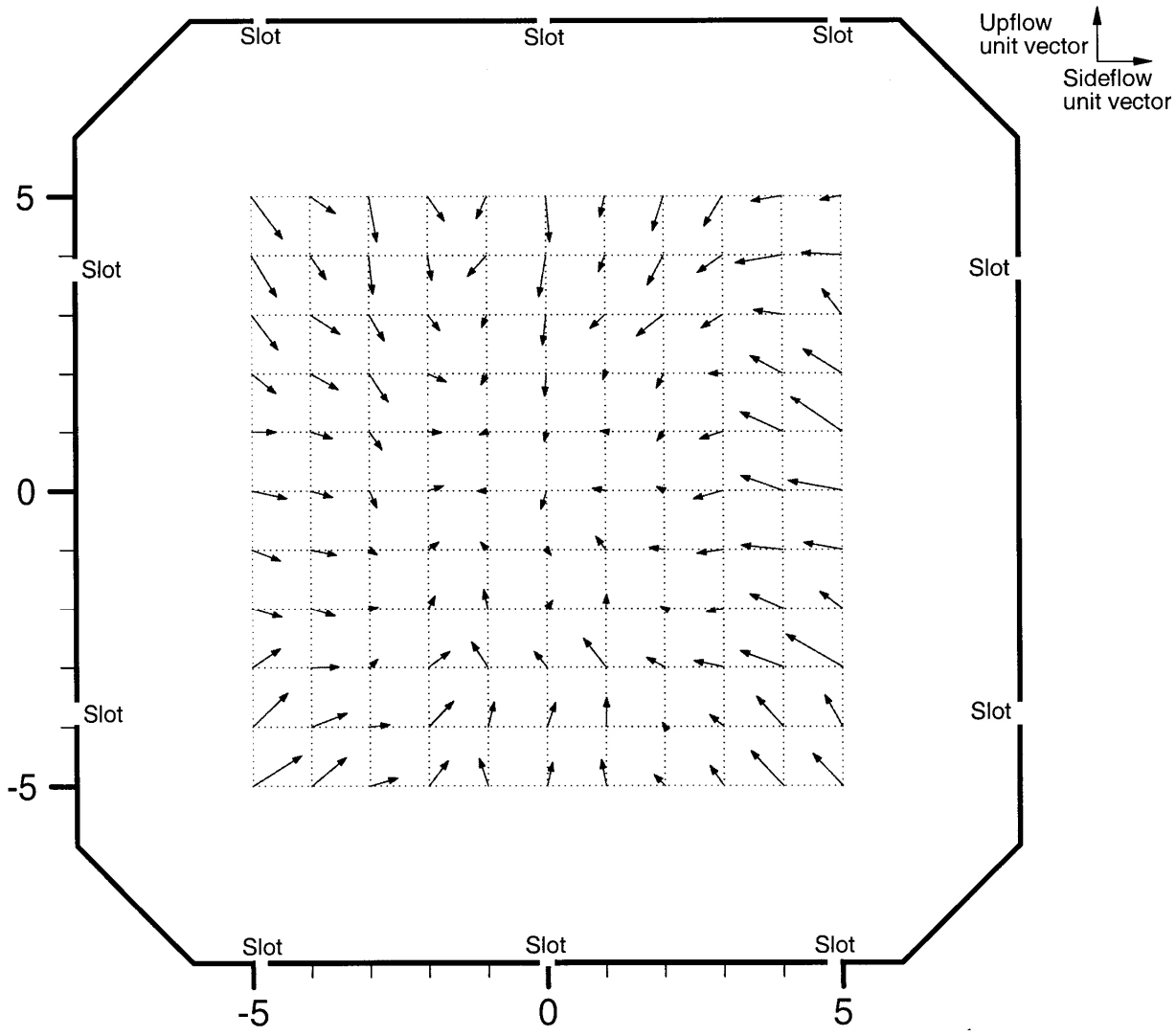

(h) M = 1.10

Figure 13. Continued.

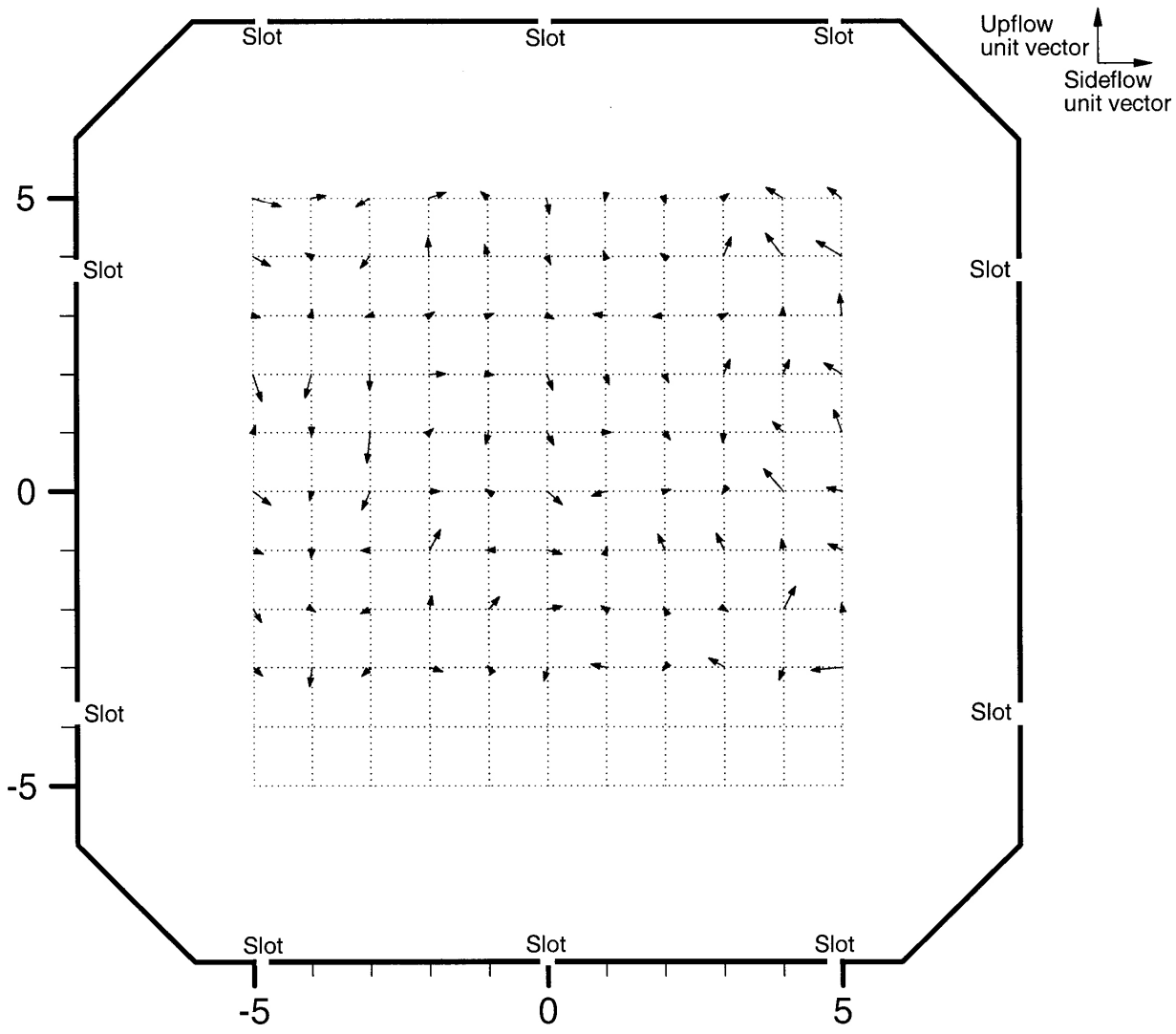

(i) M = 1.19

Figure 13. Concluded.

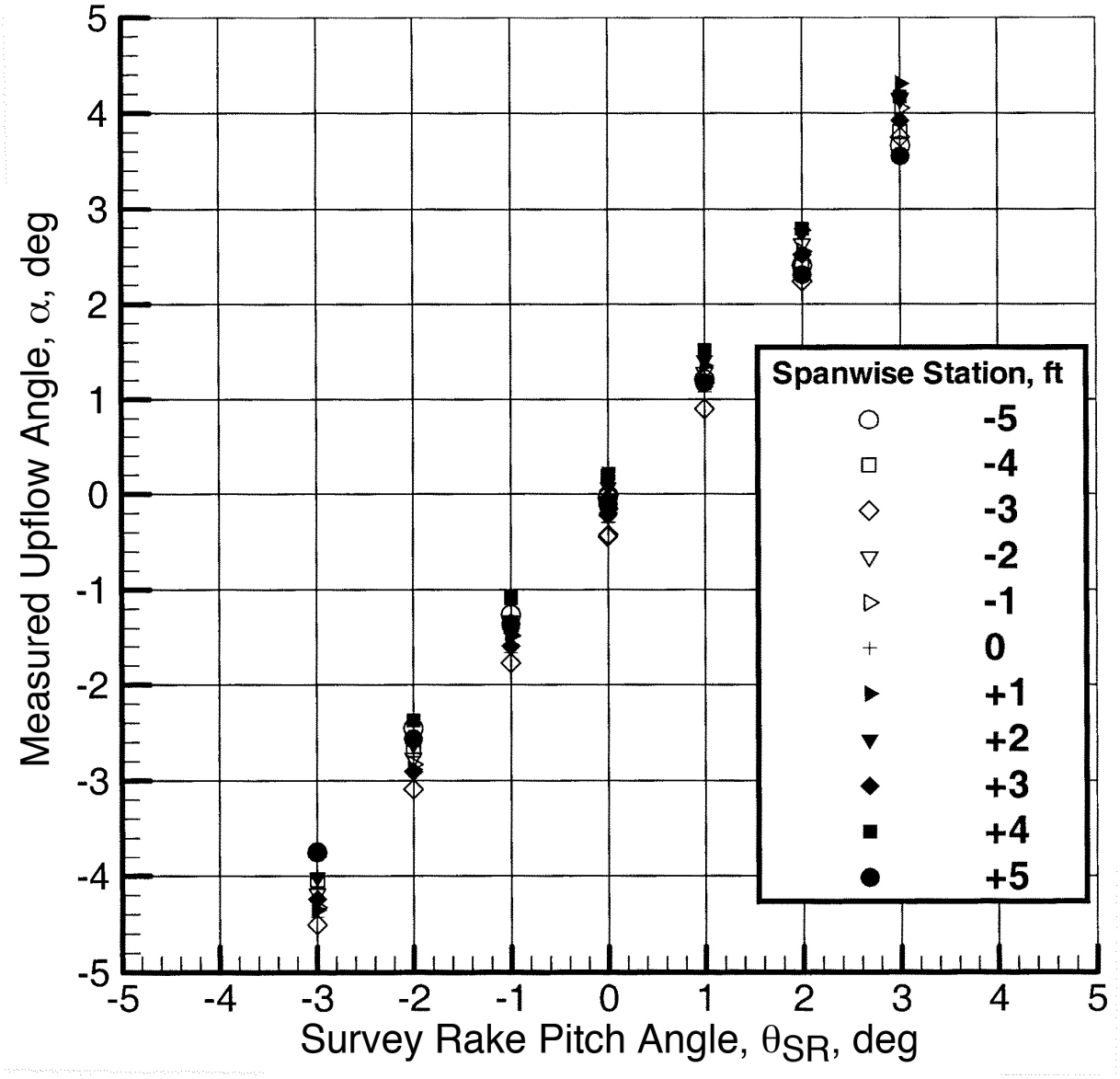

(a) M = 0.70

Figure 14. Measured upflow angle as a function of survey rake pitch angle at q = 100 psf.

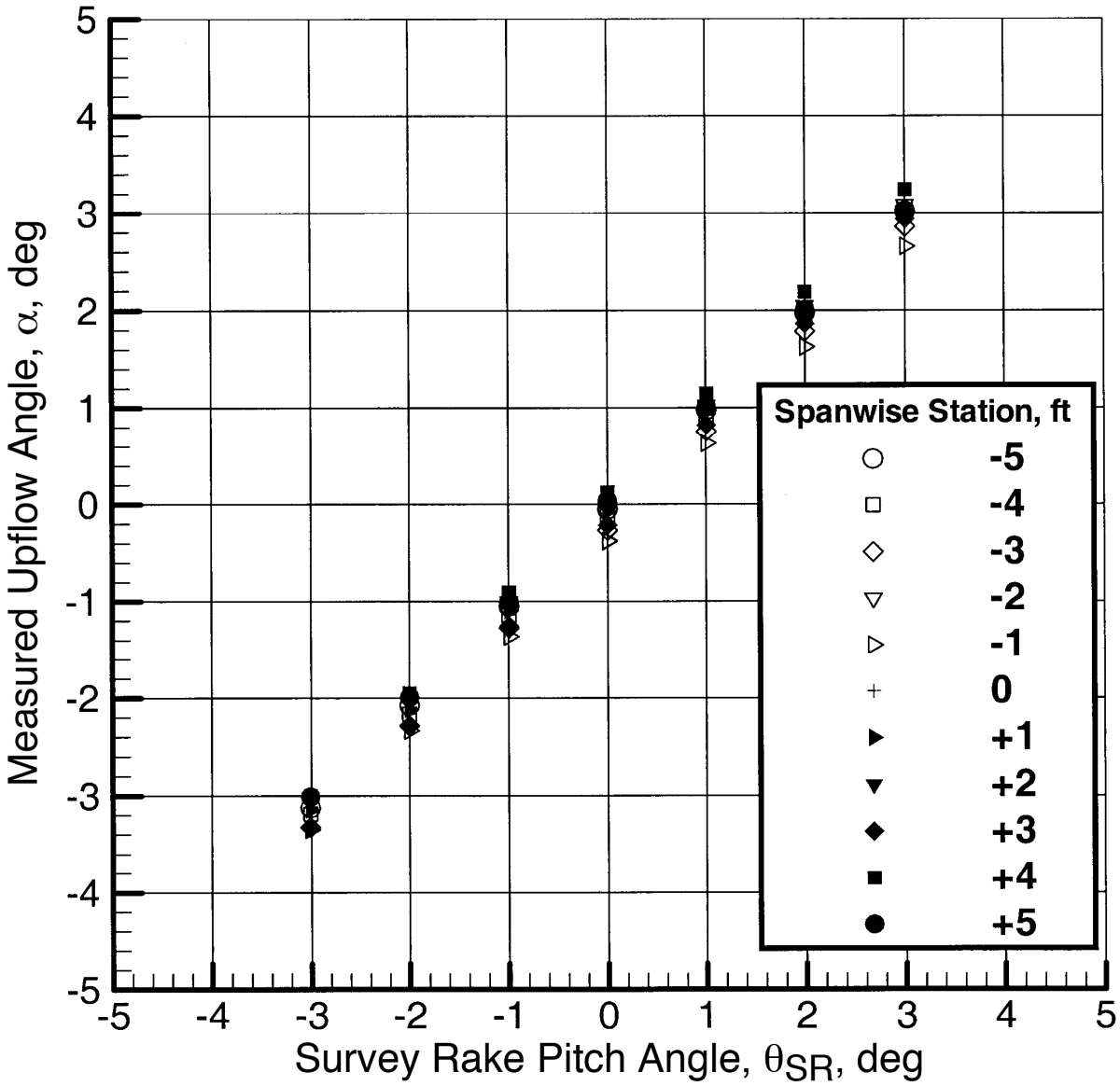

(b) M = 1.10

Figure 14. Concluded.

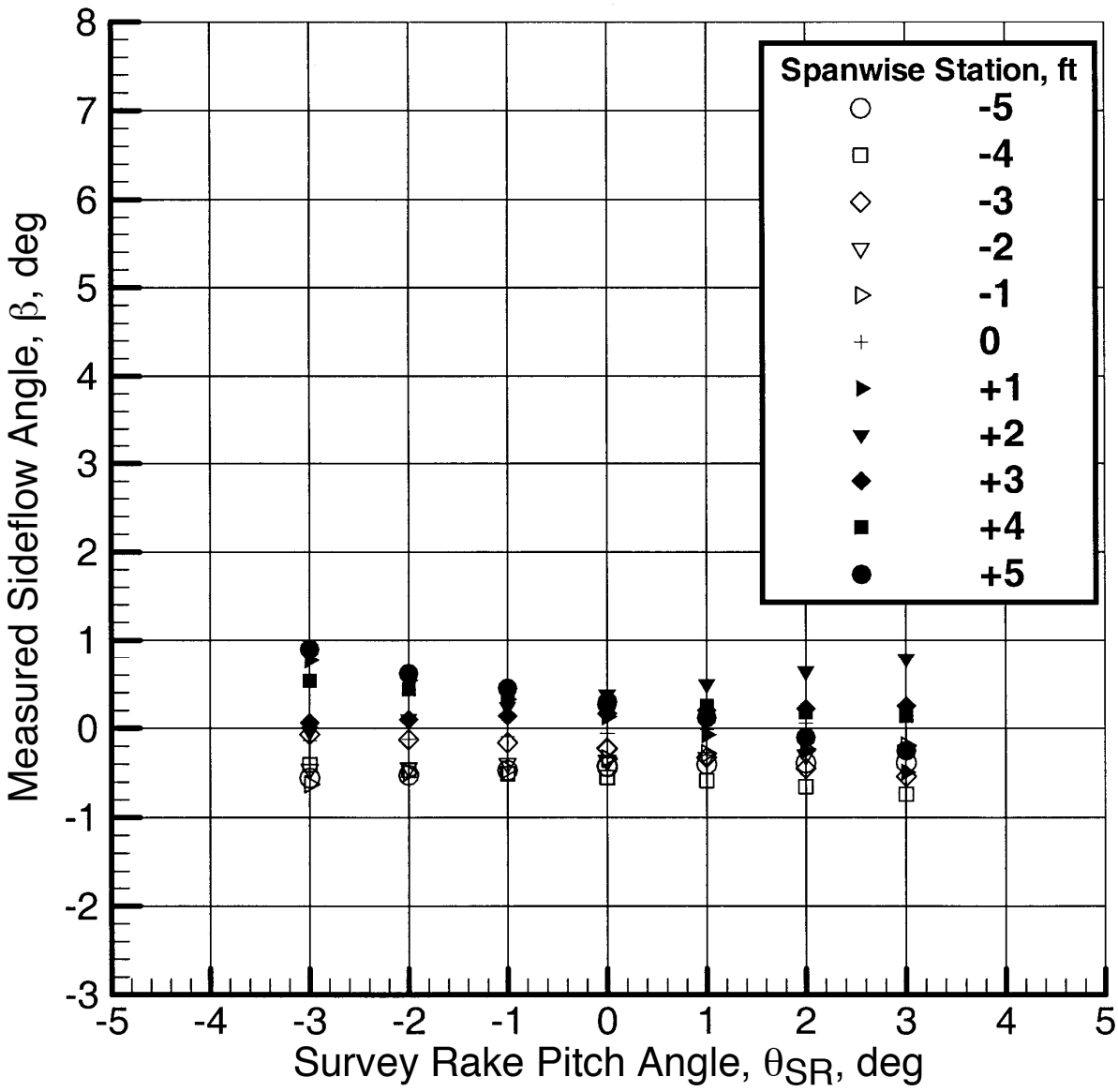

(a) M = 0.70

Figure 15. Measured sideflow angle as a function of survey rake pitch angle at q = 100 psf.

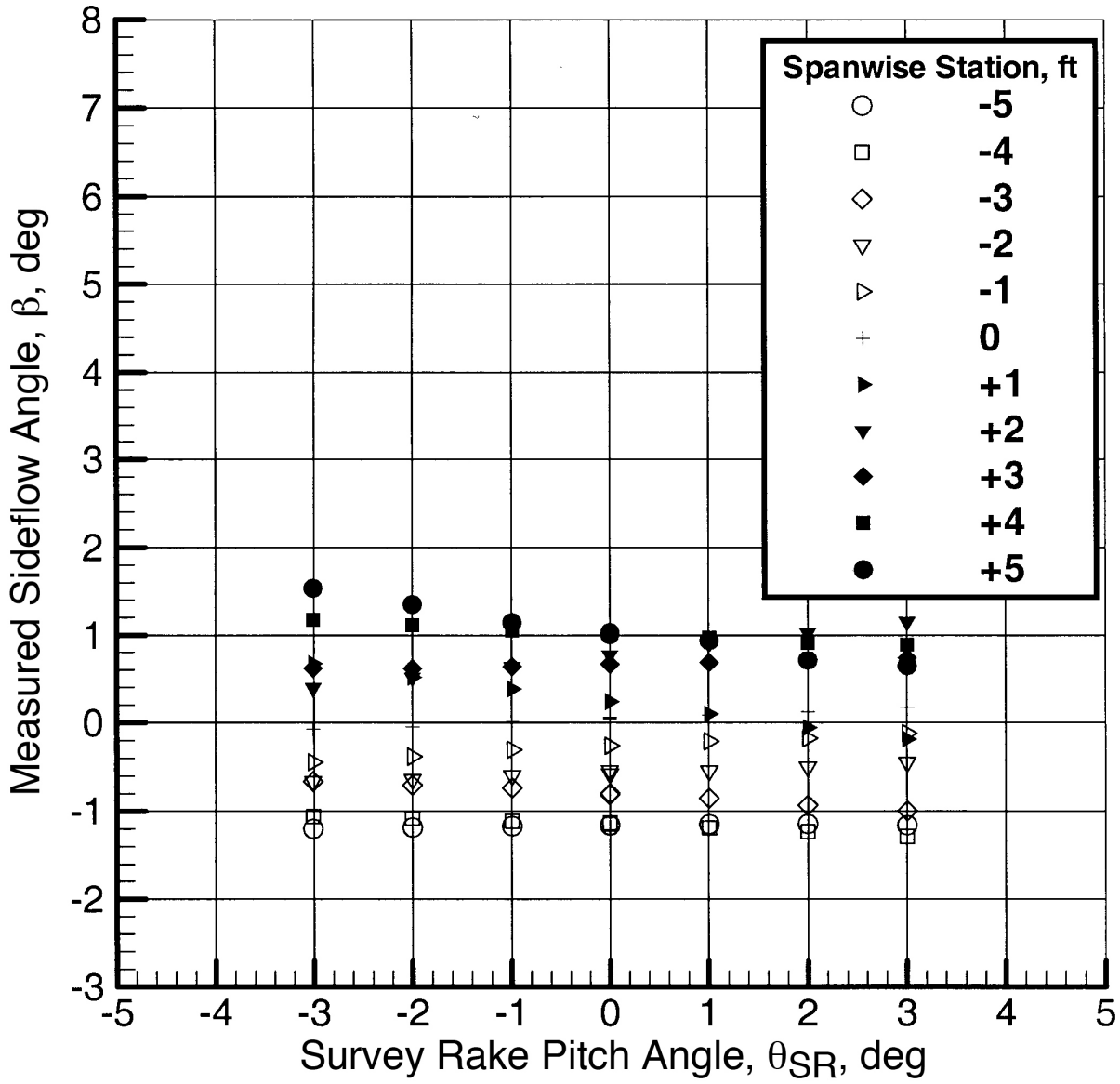

(b) M = 1.10

Figure 15. Concluded.

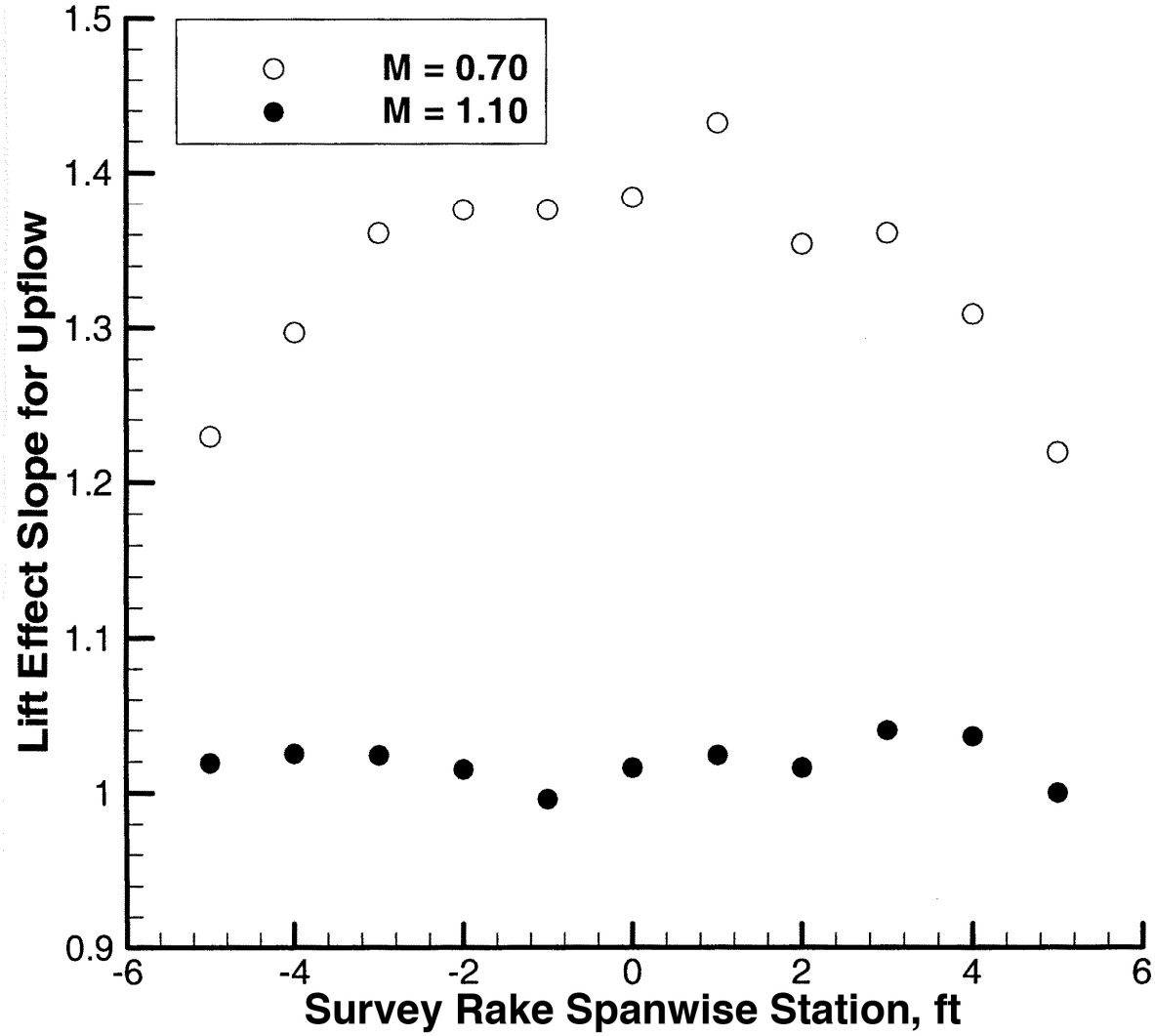

Figure 16. Calculated upflow slopes as a function of survey rake spanwise station.

REPORT DOCUMENTATION PAGE

Form Approved
OMB No. 0704-0188

1. REPORT DATE *(DD-MM-YYYY)*	2. REPORT TYPE	3. DATES COVERED *(From - To)*
01- 12 - 2005	Technical Memorandum	

4. TITLE AND SUBTITLE

Flow Angularity Measurements in the NASA-Langley Transonic Dynamics Tunnel

5a. CONTRACT NUMBER

5b. GRANT NUMBER

5c. PROGRAM ELEMENT NUMBER

6. AUTHOR(S)

Yeager, William T., Jr.; Wilbur, Matthew L.; Mirick, Paul H.; and Rivera, José A.

5d. PROJECT NUMBER

5e. TASK NUMBER

5f. WORK UNIT NUMBER

561581.02.08

7. PERFORMING ORGANIZATION NAME(S) AND ADDRESS(ES)

NASA Langley Research Center
Hampton, VA 23681-2199

U.S. Army Research Laboratory
Vehicle Technology Directorate
NASA Langley Research Center
Hampton, VA 23681-2199

8. PERFORMING ORGANIZATION REPORT NUMBER

L-19195

9. SPONSORING/MONITORING AGENCY NAME(S) AND ADDRESS(ES)

National Aeronautics and Space Administration
Washington, DC 20546-0001 and
U.S. Army Research Laboratory
Adelphi, MD 20783-1145

10. SPONSOR/MONITOR'S ACRONYM(S)

NASA

11. SPONSOR/MONITOR'S REPORT NUMBER(S)

NASA/TM-2005-213946 ARL-TR-3691

12. DISTRIBUTION/AVAILABILITY STATEMENT

Unclassified - Unlimited
Subject Category 05
Availability: NASA CASI (301) 621-0390

13. SUPPLEMENTARY NOTES

An electronic version can be found at http://ntrs.nasa.gov

14. ABSTRACT

An investigation using a survey rake with 11 five-hole pyramid-head probes has been conducted in the Langley Transonic Dynamics Tunnel (TDT) to measure the test section flow angularity. Flow measurements were made in a 10-ft square grid cenered about the test section centerline at a single streamwise location for nine Mach numbers ranging from 0.50 to 1.19 at dynamic pressures of 100 and 225 pounds per square foot. Test section flow angularity was found to be minimal with a generally random flow pattern. Corrections for survey rake induced in-plane flow were determined to be necessary; however, corrections for rake induced lift effects were not required.

15. SUBJECT TERMS

Wind-tunnel; Flow measurements; Flow angularity; Transonic Dynamics Tunnel; Calibration

16. SECURITY CLASSIFICATION OF:			17. LIMITATION OF ABSTRACT	18. NUMBER OF PAGES	19a. NAME OF RESPONSIBLE PERSON
a. REPORT	b. ABSTRACT	c. THIS PAGE			STI Help Desk (email: help@sti.nasa.gov)
					19b. TELEPHONE NUMBER *(Include area code)*
U	U	U	UU	61	(301) 621-0390